Journal Pre-proof

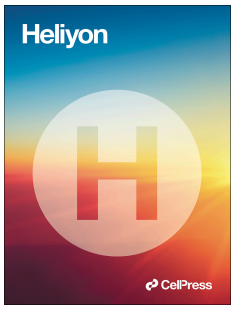

Experimental and theoretical study of improved mesoporous titanium dioxide perovskite solar cell: The impact of modification with graphene oxide

Chou-Yi Hsu, H.N.K. AL-Salman, Hussein H. Hussein, Nizomiddin Juraev, Zaid H. Mahmoud, Saeb Jasim Al-Shuwaili, Hanan Hassan Ahmed, Ahmed Ali Ami, Nahed Mahmood Ahmed, Seitkhan Azat, Ehsan kianfar

PII: S2405-8440(24)02664-1

DOI: https://doi.org/10.1016/j.heliyon.2024.e26633

Reference: HLY 26633

To appear in: *HELIYON*

Received Date: 15 January 2024

Revised Date: 16 February 2024

Accepted Date: 16 February 2024

Please cite this article as: , Experimental and theoretical study of improved mesoporous titanium dioxide perovskite solar cell: The impact of modification with graphene oxide, *HELIYON* (2024), doi: https://doi.org/10.1016/j.heliyon.2024.e26633.

This is a PDF file of an article that has undergone enhancements after acceptance, such as the addition of a cover page and metadata, and formatting for readability, but it is not yet the definitive version of record. This version will undergo additional copyediting, typesetting and review before it is published in its final form, but we are providing this version to give early visibility of the article. Please note that, during the production process, errors may be discovered which could affect the content, and all legal disclaimers that apply to the journal pertain.

© 2024 Published by Elsevier Ltd.

Journal Pre-proof

Experimental and theoretical study of improved mesoporous titanium dioxide perovskite solar cell: The impact of modification with graphene oxide

Chou-Yi Hsu[1], H. N. K. AL-Salman[2], Hussein H. Hussein[2], Nizomiddin Juraev[3,4], Zaid H. Mahmoud[*5], Saeb Jasim Al-Shuwaili[6], Hanan Hassan Ahmed[7], Ahmed Ali Ami[8], Nahed Mahmood Ahmed[9], Seitkhan Azat[10], Ehsan kianfar[†11]

[1]Department of pharmacy, Chia Nan University of Pharmacy and Science, Tainan, Taiwan

[2]Pharmaceutical Chemistry Department, college of Pharmacy, University of Basrah, Iraq.

[3]Researcher, Faculty of Chemical Engineering, New Uzbekistan University, Tashkent, Uzbekistan.

[4]Scientific and Innovation Department, Tashkent State Pedagogical University, Tashkent, Uzbekistan.

[5]University of Diyala, college of sciences, chemistry department, Iraq.

[6]Department of Medical Laboratories Technology/Al-Hadi University College, Baghdad,10011, Iraq.

[7]Department of Pharmacy, Al-Noor University College, Nineveh, Iraq.

[8]Department of Medical Laboratories Technology/ Al-Nisour University College/ Baghdad/ Iraq.

[9]college of pharmacy/National University of Science and Technology, Dhi Qar, Iraq.

[10]Satbayev University, Satbayev Str. 22a, 050013 Almaty, Kazakhstan.

[*] Corresponding author: zaidhameed_91@yahoo.com.

[†] Corresponding author: ehsan_kianfar2010@yahoo.com and ehsankianfar775@gmail.com.

Journal Pre-proof

[11]Young Researchers and Elite Club, Gachsaran Branch, Islamic Azad University, Gachsaran, Iran.

Journal Pre-proof

Journal Pre-proof

Experimental and theoretical study of improved mesoporous titanium dioxide perovskite solar cell: The impact of modification with graphene oxide

Abstract

The present study serves experimental and theoretical analyses in developing a hybrid advanced structure as a photolysis, which is based on electrospun Graphene Oxide-titanium dioxide (GO-TiO_2) nanofibers as an electron transfer material (ETMs) functionalized for perovskite solar cell (PVSCs) with GO. The prepared ETMs were utilized for the synthesis of mixed-cation (FAPbI3)0.8(MAPbBr3)0.2. The effect of GO on TiO_2 and their chemical structure, electronic and morphological characteristic were investigated and discussed. The elaborated device, namely ITO/Bl-TiO_2/3wt.% GO-TiO2/(FAPbI3)0.8(MAPbBr3)0.2/spiro-MeTAD/Pt, displayed 20.14% disposition and conversion solar energy with fill factor (FF) of 1.176%, short circuit current density (Jsc) of 20.56 mA/cm^2 and open circuit voltage (VOC) 0.912 V. The obtained efficiency is higher than titanium oxide (18.42%) and other prepared GO-TiO_2 composite nanofibers based ETMs. The developed materials and device would facilitate elaboration of advanced functional materials and devices for energy storage applications.

Keywords: Solar cell; perovskite; electron transfer material; electrospun nanofibers; mesoporous; graphene oxide.

Journal Pre-proof

1. Introduction

Recently, perovskite solar cells (PVSCs) have attracted huge attention due to the fast-growth of 3.8%–25.2% power conversion efficiency (PCE) within a very short period, which now compete with the silicon photovoltaics [1]. Organic-inorganic perovskites have been consistently attracting attention of the scientists and engineers alike in the photovoltaic society in view of their extraordinary features, e.g. long diffusion length and carrier lifetimes [2], such that the maximum conversion in this type of device approached 25.5% [3]. To improve their efficiency, some various methods or strategies were followed, e.g. the carrier multiplication impact, to get the more energy of photon with the energy larger than bandgap and multijunction absorbers to get photons with smaller energy than bandgap [4]. Presently, two kinds of architectures are known and practiced in solar cells. The first is a solar cell with a layer of mesoporous (mp) electron transport contain from semiconductor metal oxide such as TiO_2. The second type works on the basis of position of electrons and holes transporting within cell structure, which is classified as of p-i-n or n-i-p junction planer structure [5-6]. Particularly, for the solar cell with mesostructured, a solution-treated methylammonium lead iodide ($CH_3NH_3PbI_3$) shows diffusion length of electron (e^-) and hole (h^+) of 100 and 130 nm approximately. Recently, by using electron beam induced current imaging method, Edri et al., illustrated that the diffusion length of hole is longer than that of electron in titanium oxide (TiO_2) based electron transport layers [7]. Typically, TiO_2 has been employed in designing mesoporous electron transport layer (mp-ETL)[91-92]. However, the recombination of charges in mesoporous TiO_2 based electron transport layer is still remains a challenge as it inhibits the transfer of electron because of the scattering of grain boundary, which limits conversion of energy [8-14]. Therefore, enhancing the transport of charge has become an acquisition interest. For the mesostructured cells, many

endeavors have been made to expedite transport of charges via using incorporated TiO_2 or substituting it by diverse ions such as Al^{3+}, Nb^{5+}; while morphology change to nanowires TiO_2, rods and fibers was also studied [15-18]. On the other side, graphene oxide (GO) has an uncommonly high mobility of electron, high lucidity at room temperature, and higher stability, which makes it an appropriate substitute to enhance the overall efficiency of conversion for energy devices such as photochemical cells, supercapacitor and batteries [19,46-52]. Thus, GO has been utilized in various layers of PVSCs, like in mesoporous TiO_2 or even utilized in hole transfer materials [68-72]. Cho [20,53-58] served rGO-TiO_2 as a layer in PVSCs and enhanced Open Circuit Voltage (VOC) and Fill Factor (FF), resulting in high efficiency with 19.54% PCE. Wong [21] reported the use of GO-TiO_2 layers in PVSCs working under low temperature processes with 15.6% PCE. There are several more examples of using GO-TiO_2 inducing positive effects on PVSCs performance [59-63]. From above literature, it is evident that use of of GO could enhance the electronic properties of electron transfer materials [64-69]. Between all precipitation methods, electrospinning has engaged more interest because of its ability to synthesize nanoparticles with high aspect and porous [73]. Moreover, electrospinning method ease the short fabrication time, nanomaterial can be regulated easy and ecofriendly, mainly considered in biomedical engineering [74,81-83].

Herein, we aim to show a performance enhancement of mesostructured PVSCs by using GO/mp-TiO_2 as electron transport layer (ETL) with $(FAPbI_3)_{0.8}(MAPbBr_3)_{0.2}$ perovskite absorber used for effective PVSCs. The impact of GO on the performance of perovskite solar cell was estimated via time-resolved photoluminescence and ephemeral measurements. Furthermore, that the performance of GO/TiO_2 through reducing the interfacial resistance was compared with that of mp-TiO_2, as measured in terms of improvement in the efficacy of charge collection.

2. Experimental

2.1 Materials

Titanium isopropoxide, methyl amine, diethyl ether and acetic acid were supplied from Merck Co., while the polyvinylpyrrolidone (PVP, M.wt 16000), 2,2-,7,7-tetrakis-(N,N-di-p-methoxyphenyl-amine)-9,9-, formamidine acetate, chlorobenzene, hydroiodic acid, hydrobromic acid, bis (trifluoromethane) sulfonamide lithium salt, 4-tert-butylpyridine and ethanol were purchased from Sigma Aldrich(99%). All the aforementioned chemicals were used without future purification. Fluorine tin oxide conductive glass sheets was supplied by Pilkington Co.

2.2 Synthesis of GO-TiO_2 nanofibers (NFs)

The synthesis of GO-TiO_2 NFs was carried out using manual electrospinning system (Fig. 1). The electrospinning system was contained from two electrodes to connect with syringe pump and rotating drum that covered by aluminum foil under 450 rpm speed. The distance between anode and cathode was 15 cm, and the feeding rate was 1 ml/h and the applied voltage between the tip needle to rotating is 9 kV. Initially, in 3 ml absolute ethanol, 5 mg of GO was dispersed by using ultrasonication process [22-23]. After that, it was mixed with 50 ml of colloidal yellow TiO_2-PVP ethanolic viscous solution. Then, the mixture was transferred carefully to the syringe pump connected with positive electrode, while the negative electrode was linked with rotating drum. The obtained PVP-GO-TiO_2 NFs precipitated on the covered aluminum foil. Finally, it strictly removed via pointed force and calcined at 400 ^oC for 1 h donated at GO-TiO_2 NFs. The same experimental process was repeated to prepare different weight ratio of GO-TiO_2 designated as 3wt.% GO-TiO_2 and 5wt.% GO-TiO_2. The TiO_2 and GO-TiO_2 were prepared in required quantity of ethanol and ethyl cellulose and utilized for spin coating. The thickness of paste was controlled via ethanol dilution and spin coating. In present experiments, the optimized conditions

were coated via 4500 rpm for 30 sec with volume ratio of 1:5 v/v. Finally, prepared samples calcined at 550 ^{o}C for 1 h and cooled at room temperature.

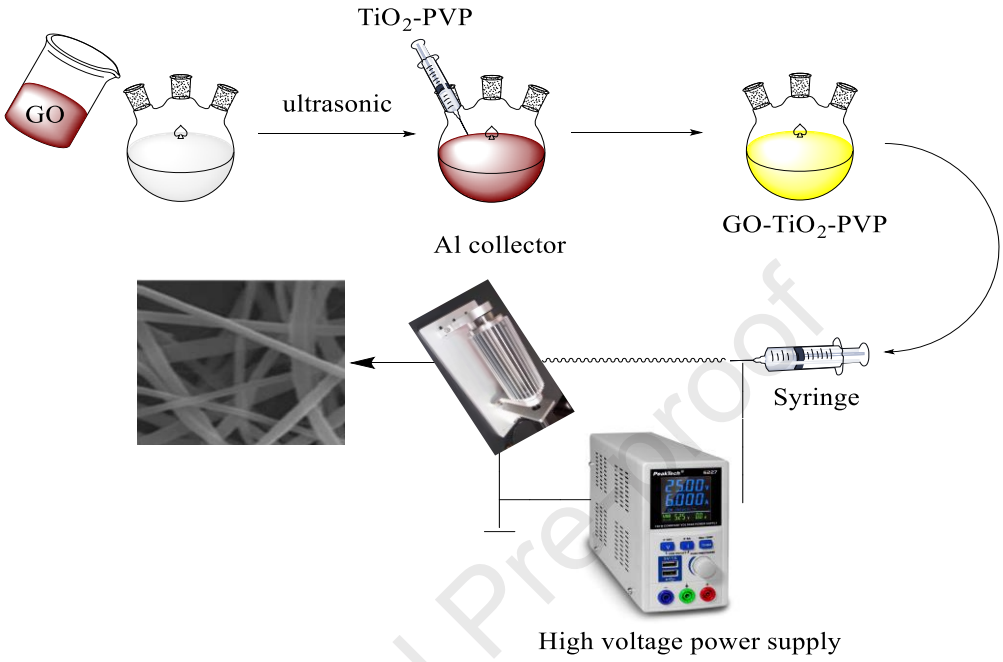

Fig. 1 Schematic of preparation of electrospun GO-TiO_2 NFs.

2.3 Device fabrication

The indium tin oxide (ITO) conductor glass with dimension 3×2 was ultrasound in absolute ethanol for 30 min before rinsed and dried using hot air flow. The carbon-titanium dioxide (C-TiO_2) was precipitated on the ITO conductive side as follows: the solution was prepared via mixing 10ml absolute ethanol, 1ml titanium chloride and 0.5 sulphuric acid (98%). Then, ultrasonic it for 1h, and was coated on the ITO substrate at 3000 rpm for 2 min using spin coating process. After that, it was dried for 1h at room temperature for 30 min, and posteriorly burned at 500^{o}C for 1h to prompt the crystallization. The layer of 0.01%wt. GO/TiO_2 was precipitated on the C-TiO_2 layer as follow: the precursor solution of 0.04%wt. GO/TiO_2 was prepared via mixing TiO_2, GO and absolute ethanol (1:4wt./wt. ratio). The solution was

ultrasound for 30 min and spin-coated (0.1ml) on the layer of TiO_2 at 300rpm for 1 min, and then heated it at 250 ^oC for 1h. To obtain perovskite $(FAPbI_3)_{0.8}(MAPbBr_3)_{0.2}$ layer, a method with one step was done under N_2 conditions. In 100ml of DMSO/DMF solvents, Formamidinium iodide (FAI) prepared by condensing 30 ml HI with 14g of $C_3H_8N_2O_2$, methylammonium lead bromide prepared by condensing 5ml HBr with 40wt.% methyl amide, lead iodide and lead bromide were mixed together under ice condition. The mix solution was spin-coated on 0.01 %wt. GO/TiO_2 layer at 5000 rpm through 60 sec and followed via drying at 80 ^oC for 1 h. For (spiro-OMeTAD) layer, 0.16 g of 2,2$^-$,7,7$^-$-tetrakis-(N,N-di-p-methoxyphenyl-amine)-9,9$^-$-spirobifluorene in 2 ml chlorobenzene, 76 ml of bis (trifiuoromethane) sulfonamide lithium salt in 30 ml 4-tert-butylpyridine was mixed with strong stir for 2h. The (spiro-OMeTAD) solution was spin-coated at 4000 rpm for 1 min and leave it for 3h to enhance the conductivity. Finally, the prepared device was carried to chamber of vacuum evaporation (1×10^{-6} torr) for precipitation of Pt contact that prepared by photolysis method [24-26,84-90] previously. The temperature of chamber was maintained unchanged by putting the source material in contact with a hot surface, that was resistively heated by passing a current through it. The fabricated process was summarized in Fig. 2.

Journal Pre-proof

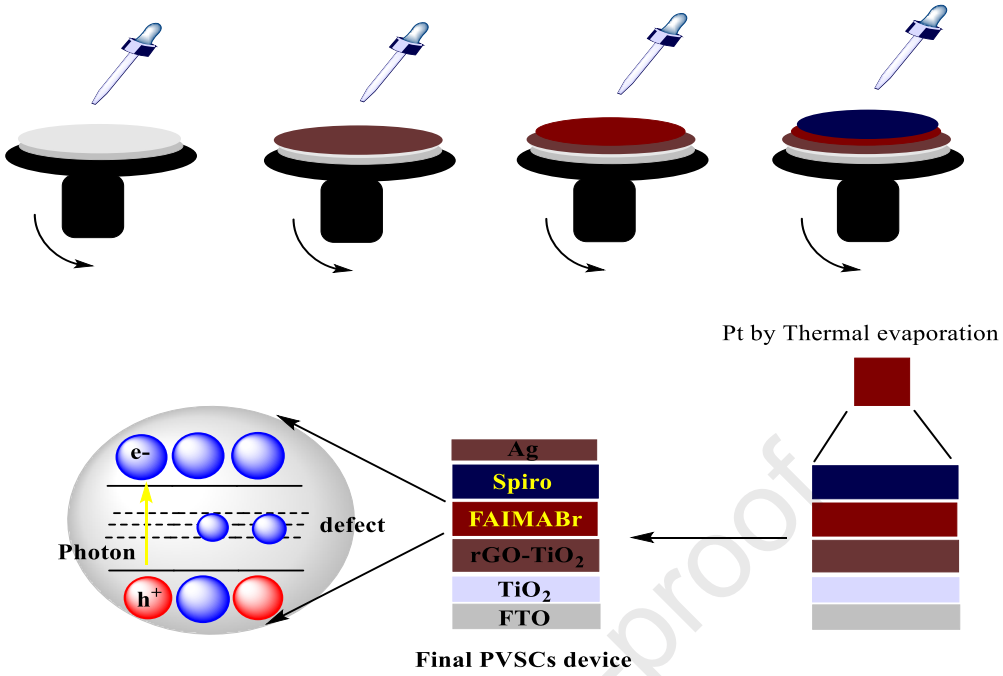

Fig. 2. Steps taken in the fabrication of PVSCs.

2.4 Theoretical details

The PVSC with (n-i-p) configuration (ITO/TiO_2/GO-TiO_2/$(FAPbI_3)_{0.8}(MAPbBr_3)_{0.2}$/spiro-OMeTAD/Pt) utilized for numerical emulation is demonstrated in Fig. 3a. A model explanation of a cross section with each layer for (ITO/TiO_2/GO-TiO_2/$(FAPbI_3)_{0.8}(MAPbBr_3)_{0.2}$/spiro-OMeTAD/Pt) is displayed in Fig. 3b. To comprehend the behavior of (ITO/TiO_2/GO-TiO_2/$(FAPbI_3)_{0.8}(MAPbBr_3)_{0.2}$/spiro-OMeTAD/Pt) solar cell, a theoretical study was carried out using SCAPS-1D under 25 ^{o}C and AM 1.5 solar spectrum and compared the experimental results. Poisson equation was used to describe the J-V characteristics and related to the electric field of p-n junction to the density of space charge as following (Eq.1):

$$\frac{\partial^2\varphi}{\partial^2 x} = -\frac{\partial E}{\partial x} = -\frac{\rho}{\varepsilon_s} = -\frac{q}{\varepsilon_s}[p - n + N_D(x) - NA(x) \pm N_{def}(x)] \quad (1)$$

where ε_s is permittivity of static materials, φ electrostatic potential, p is hole density, q: elementary charge and n: density of electrons. At steady state, the continuity equations of electron and hole as follows (Eqs.2-3):

$$\frac{\partial J_n}{\partial x} + G - U_n(n,p) = 0 \quad (2)$$

$$\frac{-\partial J_p}{\partial x} + G - U_p(n,p) = 0 \quad (3)$$

where Jn and Jp are the electrons and holes current density, G: generation rate of electron-hole and Un and Up are the rate of net recombination.

Equations of drift diffusion (Eqs.4-5):

$$J_n = qp\mu_n E + qD_n \frac{\partial n}{\partial x} \quad (4)$$

$$J_p = qp\mu_p E - qD_p \frac{\partial p}{\partial x} \quad (5)$$

μ_n and μ_p are the mobility of electron and hole, Dn, Dp: electron and hole diffusion coefficient and q: elementary charges. For the simulation of SCAPS, the parameters need to be entered. The solar cell parameters were taken depended on previously works [27,28] and summarized in **Table. 1**.

Journal Pre-proof

Table 1. Perovskite solar cell parameters set.

Parameters	ITO	TiO_2	GO/TiO_2	perovskite	Spiro-oMeTAD
Thickness (nm)	290	30		290	220
Bandgap (eV)	3.4	3.12		1.54	3.06
Electron affinity (eV)	3.9	4		3.8	2.1
Dielectric perittivety (er)	8	9		6.2	2.8
Electron mobility (cm^2/Vs)	18	18	280	1.8	10^{-3}
Hole mobility (cm^2/Vs)	12	12		1.8	10^{-3}
Donor density (cm^{-3})	$3*10^{19}$	$2*10^{15}$		10^9	/
Acceptor density (cm^{-3})	/	/		10^9	$3*10^{19}$

2.5 Characterization

The functional groups of prepared samples were investigated utilizing Fourier transform infrared spectra (Perkin elmer, Germany), while the Raman spectra were carried out at room temperature by Raman spectrometer (Tensor II, Bruker, Germany) with excitation light source of 522 nm. The X-ray photoelectron spectroscopy measurements were determined to estimate binding energy with ESCALAB 250XI system. Crystal structure and size were characterized with Cu Kα radiation (λ = 1.5418 A^o) via X-ray diffractometer (D8 advanced, Bruker, Germany) and using Scherrer equation [29] as following (Eq.6):

$$D = 0.9\,\lambda/\beta\cos\theta \qquad (6)$$

Morphology of the prepared samples was observed on a field emission electron microscope type (S-3400N, Hitachi, Japan). The optoelectronic properties were estimated by using photoluminescence that recorded on fluorescence spectrophotometer (F-4600, Hitachi, Japan), while the time-resolved photoluminescence decay was recorded at 650 nm utilizing excitation

light pulse with 470 nm and 5 MHz frequency from F-7000 spectrophotometer. The lifetime decay was calculated [30] by using following (Eq.7):

$$I(t) = I_o + A_1 e^{(\frac{-t+t_o}{\tau 1})} + A_2 e^{(\frac{-t+t_o}{\tau 1})} \quad (7)$$

where A_1, A_2 are weight factors of decay channel, $\tau 1,2$ first and second order of decay time. The average lifetime was calculated by using the following equation (Eq.8):

$$\tau_{avg} = \sum_n \frac{\sum A_n \tau_n^2}{\sum_m A_m \tau_m^2} \quad (8)$$

3. Results and discussion

3.1 structure analysis

The structural investigations on the prepared compounds were carried out using FTIR, Raman spectra, XRD and XPS. To confirm fully oxidize of graphite to GO, FTIR analysis was carried out. The FT-IR spectrum of GO, TiO_2, and GO incorporated TiO_2 is shown in Fig. 3a-c. In Fig. 3a, a broad band located at 3410 cm^{-1} can be attributed to OH stretching vibration mode. The stretching mode of C=O is shown at 1755 cm^{-1}, while the skeleton vibration of C=C is observed at 1652 cm^{-1}. At 1395cm^{-1}, a peak is clearly appeared, which is corresponding to binding mode of C-H. Another peak is noted at 1048 cm^{-1}, which assigned to vibration of C-O [31]. The FTIR spectrum of TiO_2 anatase phase is shown in Fig. 3b. The main vibration peak is located at 625 cm^{-1}, which assigned to Ti-O bond. In spectrum of GO incorporated TiO_2 (Fig. 3c), the absorption peak is weekend, which indicate some interaction between TiO_2 and GO, as well as, reduce in adsorption peaks of O-H and C=O and become weaker, which is corresponding to some reaction.

Journal Pre-proof

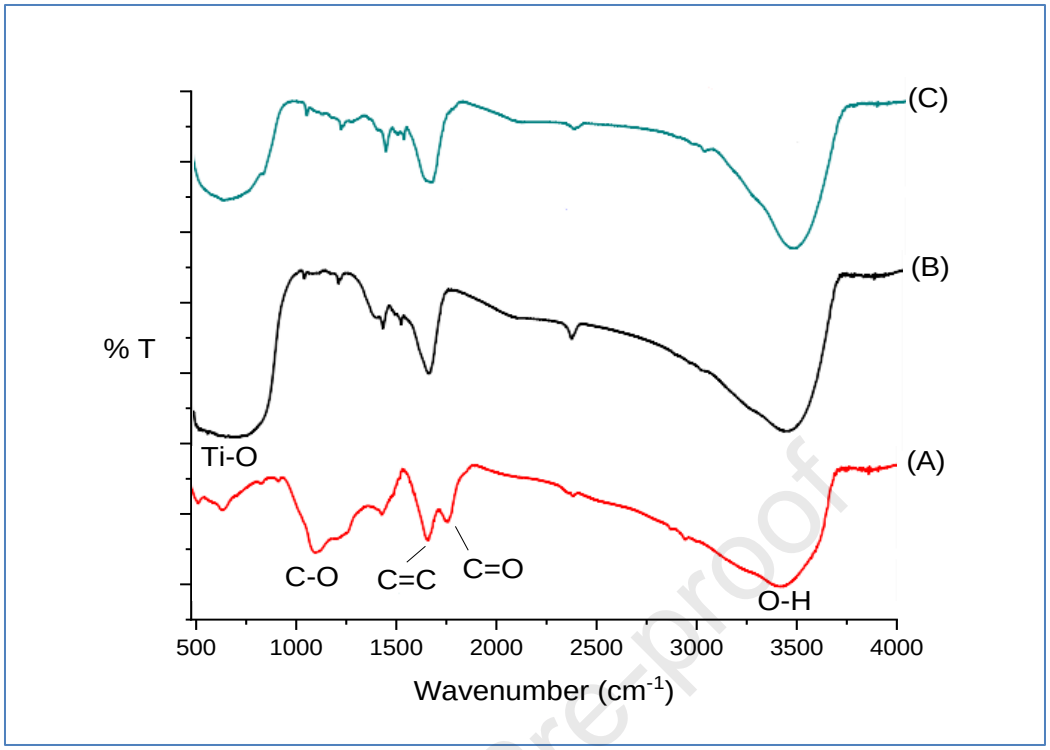

Fig. 3 FTIR of (A) GO, (B) TiO_2 and (C) 3wt.% GO-TiO_2.

The Raman spectra of GO as well as TiO_2 particles modified with 1wt.% or 3wt.% GO are shown in Fig. 4a-c. Raman spectra of all synthesized compounds are demonstrated two eminent intensity peaks centered at 1380 and 1615cm^{-1}, which assigned to D and G bands, respectively. As shown in Fig. 4b and c, four predominate intensity bands are located at 180, 425, 540 and 663 cm^{-1} which are attributed to Eg, B_1g, A_1g + B_1g and Eg active modes of anatase phase. When compared the intensity ratio ID/IG for 1wt.% and 3wt.% GO incorporated TiO_2, it is found that it increased with increase of GO dopant, which indicated formation of more carbonic structures with sp^3 hybridization. The D intensity peak is shifted to lower wavenumber with increasing TiO_2, which may be back to the stress by TiO_2 nanoparticles growing on the graphene sheet surface, this confirms more reaction or interaction between GO and TiO_2 [32-33,76-80].

Journal Pre-proof

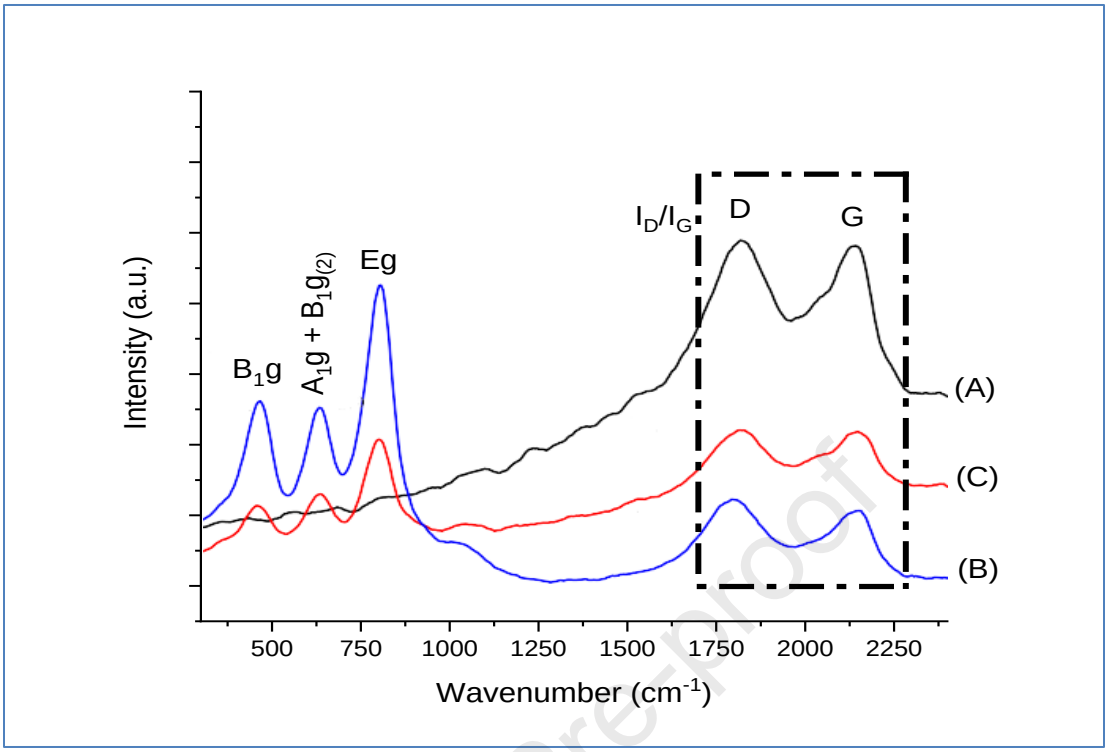

Fig. 4. Raman spectrum (A) GO, (B) 1wt.% and (C) 3wt.% GO incorporated TiO_2.

To estimate the elemental composition and chemical state, XPS analysis was carried out. The XPS analyses of GO and 1wt.% GO-TiO_2 are shown in Fig. 5a-d, in which fully element fine spectra of C 1s and O 1s can be distinctly specified. The fine spectra of O 1s in GO and 1wt.% GO-TiO_2 are also shown in Fig. 5b. The XPS analysis shows difference in peak position and shapes. For GO, the intensity peak at 533 eV is imputed to OH groups on the surface (Fig. 5b), while the intensity peak at 530 eV can be corresponding to Ti-O-C bond for 1wt.% GO-TiO_2 and this bonding refers to strong interaction between GO and TiO_2 that been product from incorporating process [34]. The C 1s intensity peak of GO and 1wt.% GO-TiO_2 are demonstrated in Fig. 5c. The results indicated that the binding energy C 1s for 1wt.% GO-TiO_2 is lower than in GO. Moreover, it appears two peaks at 286 and 288 eV which assigned to C-C and C=C of pure GO, while intensity peak centered at 284 eV corresponds to C-O of 1wt.% GO-TiO_2. Fig. 5d shows deconvolution curves of C 1s for pure GO and 1wt.% GO-TiO_2. The peaks located at 286,

288 and 290 eV are respectively corresponding to C-C, C-O and O-C=O bonds of GO, while for same bonds in 1wt.% GO-TiO_2, it showed at 284, 286 and 288 eV [35]. As illustrated obviously in XPS spectra, the intensity strength of oxygen functional group reduced clearly in 1wt.% GO-TiO_2 indicating reducing it after incorporation process.

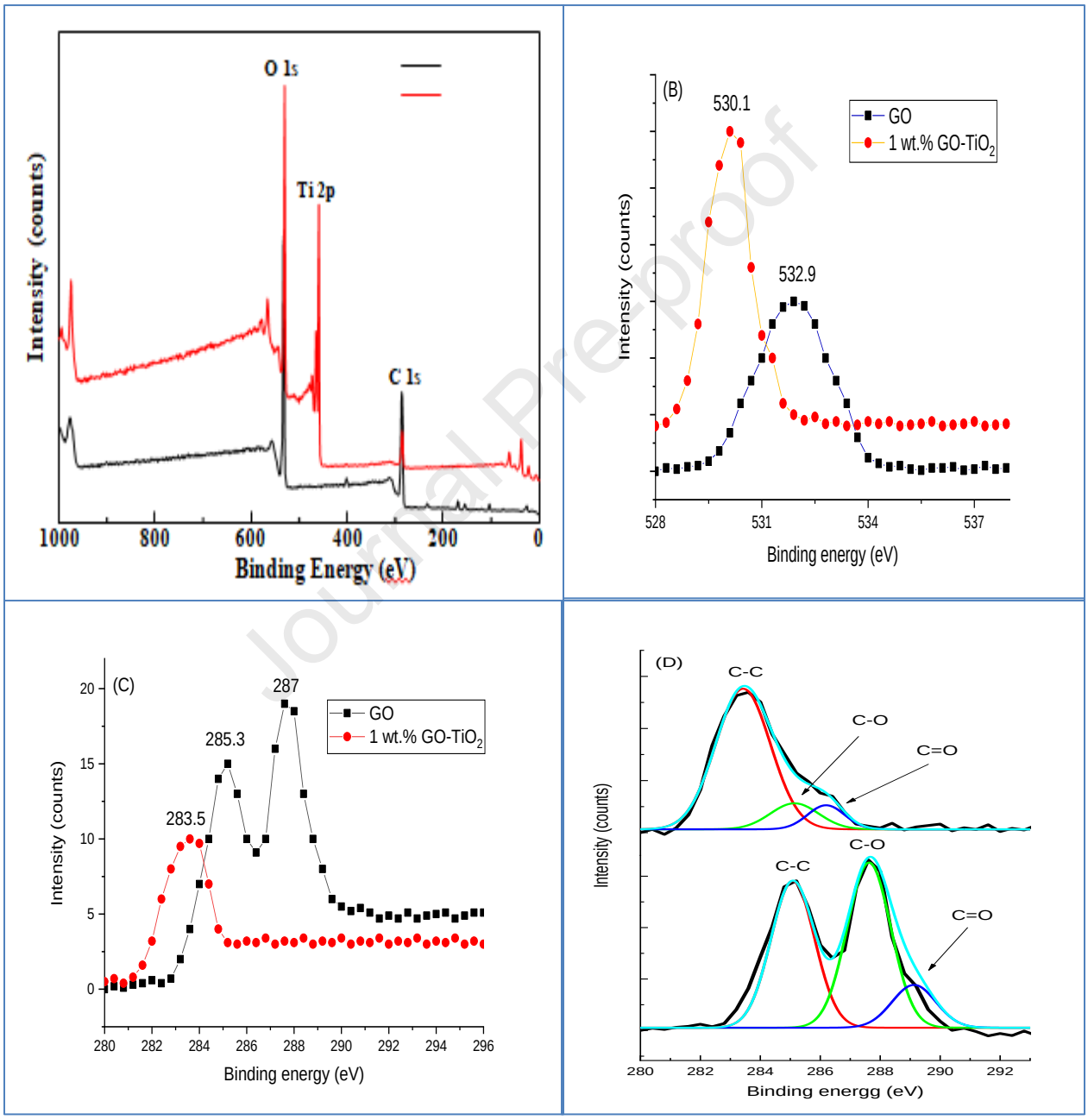

Journal Pre-proof

Journal Pre-proof

Fig. 5. XPS of GO and 1wt.% GO-TiO_2 (a) survey spectrum, (b) O 1s, (c) C 1s, and (d) deconvoluted C 1s.

The XRD of pure GO, TiO_2 and 1, 3 and 5wt.% GO incorporated TiO_2 nanocomposite are shown in Fig. 6a-e. The diffraction peak locates at 11.7^o is assigned to GO, corresponding to the spacing of layer of graphene oxide (GO) 0.75 nm, which is larger than layer spacing of graphite that reported by Wang et al. [36]. The enlarged layer space is indicated entering oxygen-functional groups into the graphite structure, which leads to expansion of layer of graphite. The XRD pattern of TiO_2 and 1, 3 and 5wt.% GO incorporated TiO_2 are in good agreement with tetragonal anatase TiO_2, the results with (JCPDS-21-1272), diffraction peaks at 2θ of 25.35^o, 37.78^o, 48.07^o, 53.93^o, 55.11^o and 62.72^o corresponding to (101), (004), (200), (105), (211) and (204), respectively. The XRD results suggest that incorporating GO holds the anatase TiO_2 phase profitably with no obvious effect of patterns of it, as well as, the results show no obvious diffraction peaks for GO in GO-TiO_2 nanocomposite, demonstrating the relativity limited mass percentage of GO incorporating [37]. Moreover, the expanded spectra obviously appeared at (101) diffraction peak at 2θ of 25.35^o, which is progressively moving towards lower 2θ, indicating a possible reaction between GO and TiO_2 during incorporating process.

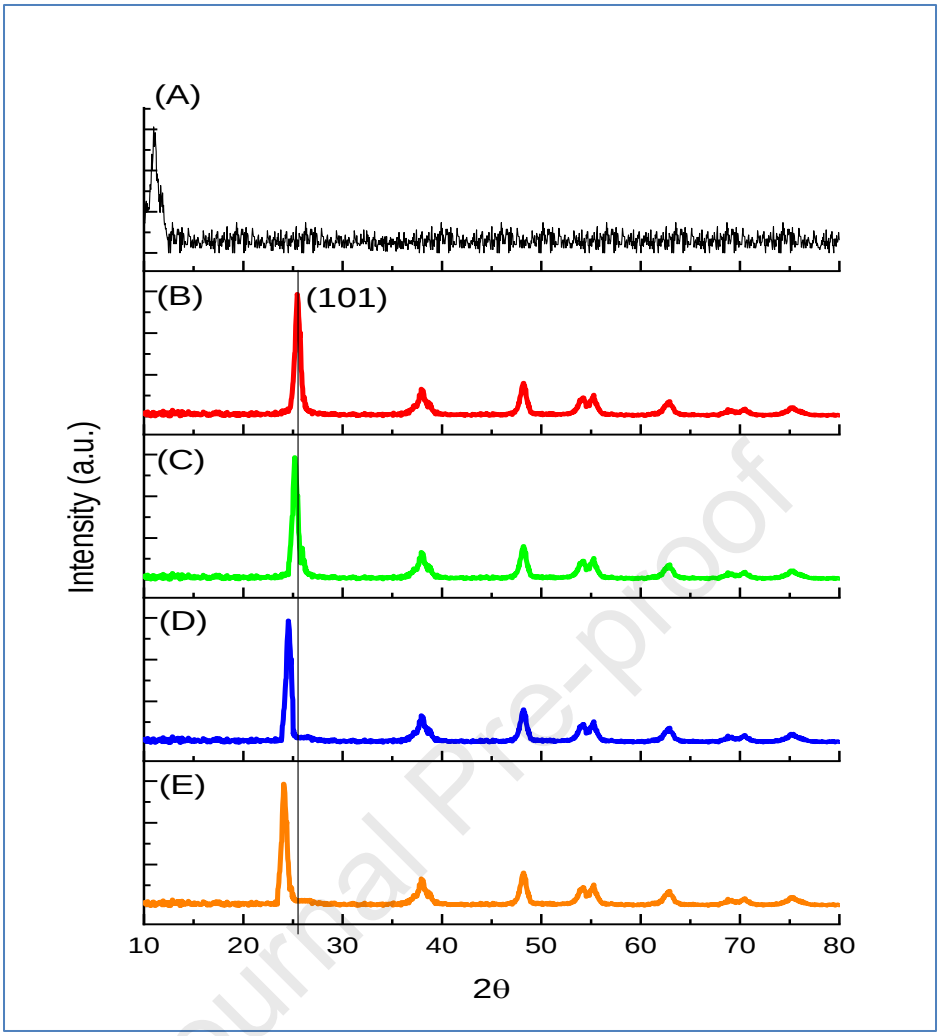

Fig. 6. XRD of (A) GO, (B) TiO_2, (C) 1wt.% GO-TiO_2, (D) 3wt.% GO-TiO_2 and (E) 5wt.% GO-TiO_2.

The XRD analysis of $(FAPbI_3)_{0.8}(MAPbBr_3)_{0.2}$ thin film precipitated via different TiO_2 and 1wt.% GO-TiO_2 electron transfer materials is shown in Fig. 7a-c. The results appear diffraction peaks at 2θ of 14.3º, 21.12º, 29.55º and 33º, respectively corresponding to (111), (120), (222) and (231), which revealed the tetragonal structure perovskite lattice [38]. On the other hand, the results exhibited slight shift towards higher positions, with respect to 2θ of (14.3º) because of deposition of $MAPbBr_3$. The XRD patterns appeared that the reflection peak at 14.3 (111) in GO-TiO_2 based perovskite film is higher than TiO_2 and it preferred (111) orientation axis.

Journal Pre-proof

Moreover, for GO-TiO_2 based perovskite film, the relative intensity of planes (111) to (120) is much higher than other film, which may be back to the vertical growth perovskite grain.

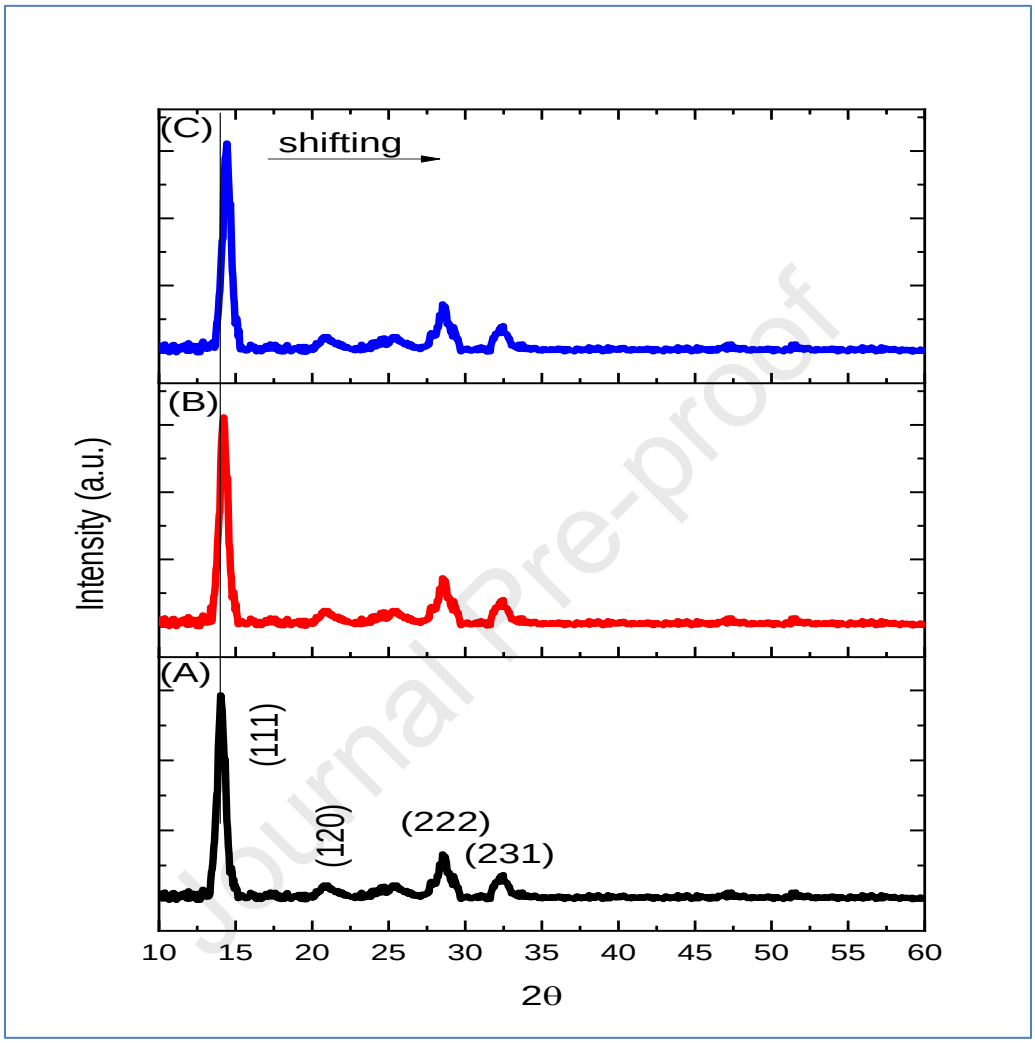

Fig. 7. XRD of (A) $(FAPbI_3)_{0.8}(MAPbBr_3)_{0.2}$, (B) TiO2 doped and (C) 1wt.% GO-TiO_2 doped.

3.2 Morphology characterization

The surface morphology of the prepared samples was estimated using FESEM-EDX and TEM. The FESEM images of GO and rGO are shown in Fig. 8a,b. The images are exposed thin sheets

with folded morphology, as well as, the GO images shown a small rolling structure and the aggregated GO sheets are straggled from one another. After reduction process (Fig. 8b), the layer of rGO becomes less carbonic, illustrating the presence of well exfoliated graphene. Moreover, the rGO SEM images demonstrated a very small thickness and random distribution [39]. Fig. 8c appears the FESEM images of TiO_2 were precipitated at 2 ml/h feed rate, which disclosed forming NFs with uniform diameter and length. The FESEM images of incorporating different weight ratio of GO with TiO_2 are exhibited in Fig. 8d-f. The images appear that the GO ratio incorporating are effect on the diameter of TiO_2 NFs clearly, whereas, the diameter of TiO_2 NFs is reduced upon increase of GO, but decreased from 135 to 230 nm. Fig. 8g-j shows the FESEM images of $(FAPbI_3)_{0.8}(MAPbBr_3)_{0.2}$ thin film precipitated on the FTO substrate, TiO_2, 3wt.% rGO-TiO_2 and 5wt.% rGO-TiO_2 respectively. The images (Fig. 8g) exhibit a consolidated and bushy or dense with 450-500 nm grain size, while Fig. 8h shows severe in grain size up to 600 nm and these boosts in grain size propose that the TiO_2 easies nucleation site for the $(FAPbI_3)_{0.8}(MAPbBr_3)_{0.2}$. When $(FAPbI_3)_{0.8}(MAPbBr_3)_{0.2}$ is precipitated on FTO/TiO_2, the grain size has been rising to 800nm approximately with consolidated in nature as shown in Fig. 8i. This increase in particle size and compact nature of grain size causes higher VOC, FF and lower recombination rate, leading to higher conversion efficiency of solar cell. Moreover, an increase in rGO incorporating ratio to 5wt.% causes slight reduction in grain size to 750 nm, but most of grain remain precise, as in Fig. 8j. These reduction in grain size emerges from high nuclei center that is produced from higher concentration of GO and smaller diameter of TiO_2 [40]. From these FESEM results, the 3wt.% rGO-TiO_2 electron transfer materials easies the less sites of nucleation. It is recognized that lower crystallization of $(FAPbI_3)_{0.8}(MAPbBr_3)_{0.2}$ perovskite layer consisted of a higher $\Delta G_{critical}$ energy, which then decreases the nuclei numbers.

Therefore, the growth of perovskite layer will begin from limited defined nuclei centers, which results in limited grain boundary and grain with large size [41-42].

Journal Pre-proof

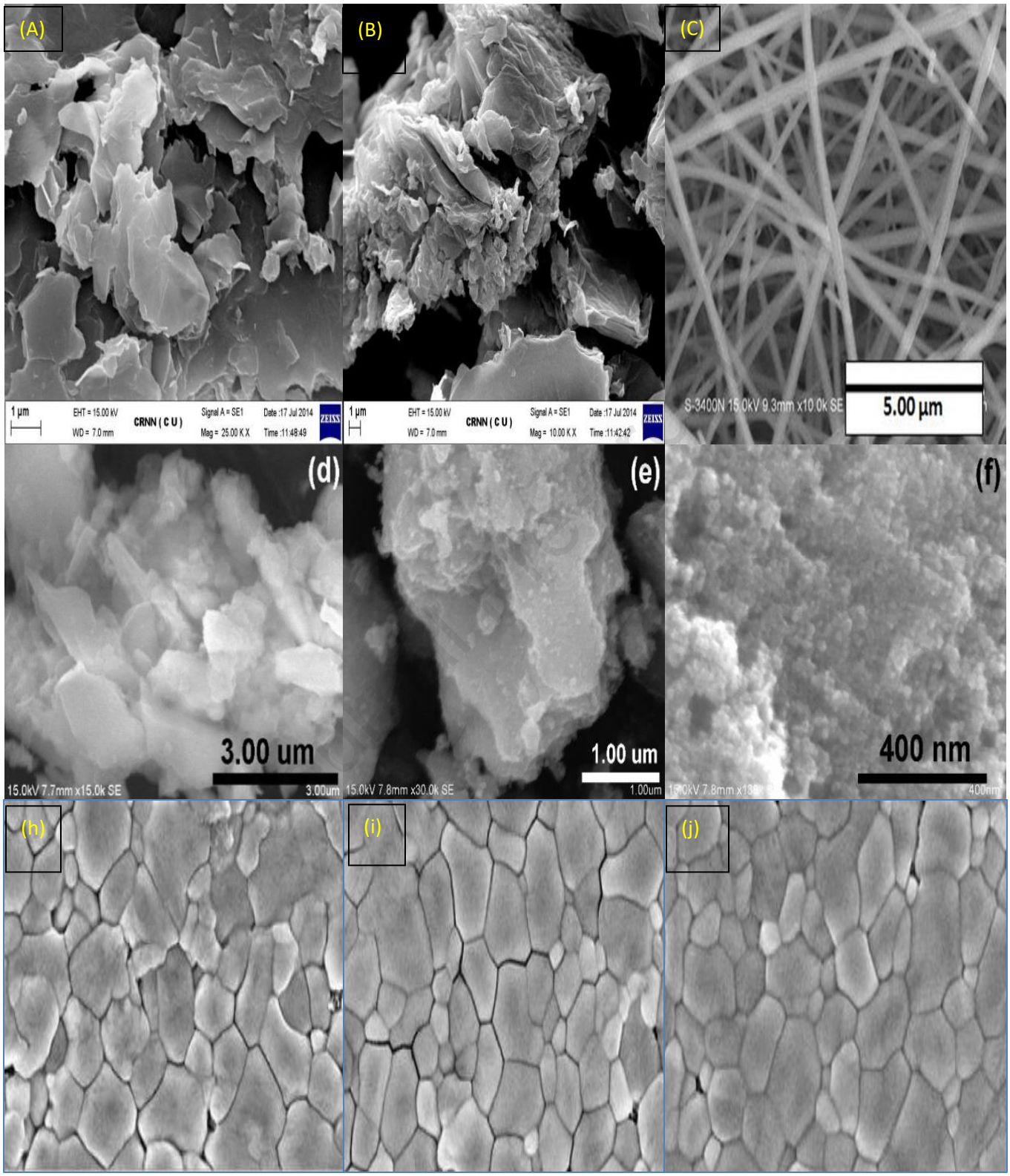

Fig. 8. FESEM of (a) GO, (b) rGO, (c) TiO_2 NFs, (d) 1 wt.% GO-TiO_2, (e) 3 wt.% GO-TiO_2, (f) 5 wt.% GO-TiO_2, $(FAPbI_3)_{0.8}(MAPbBr_3)_{0.2}$ perovskite deposited on different ETLs on (h) 1 wt.% GO-TiO_2, (i) 3 wt.%

GO-TiO_2 and (j) 5 wt.% GO-TiO_2.

3.3 Optoelectronic analysis

The photoluminescence (PL) and time-resolved photoluminescence (TRPL) analysis were carried out to estimate the optoelectronic properties and charge dynamic of TiO_2, 1 and 3wt.% GO-TiO_2 deposited on $(FAPbI_3)_{0.8}(MAPbBr_3)_{0.2}$ layer as an electron transfer material (ETMs) and the results are shown in Fig. 9 and 10. In Fig. 10, the PL spectra appeared without a hole transfer material (HTM) quencher, as well as, it showed an emission peak at ~ 778 nm back to prepared samples. The PL spectra showed emission peak at ~ 778 nm for TiO_2NFs/$(FAPbI_3)_{0.8}(MAPbBr_3)_{0.2}$ with a reduction for hybrid samples because of the effective electron disarmament from conduction band (CB) of /$(FAPbI_3)_{0.8}(MAPbBr_3)_{0.2}$ to CB of GO and then to TiO_2. In addition to, the PL intensity of the produced nanoparticles dropped when the concentration of GO increased, showing a delay or friction in electron–hole recombination due to effective charges transfer as the doping ratio was increased.

Journal Pre-proof

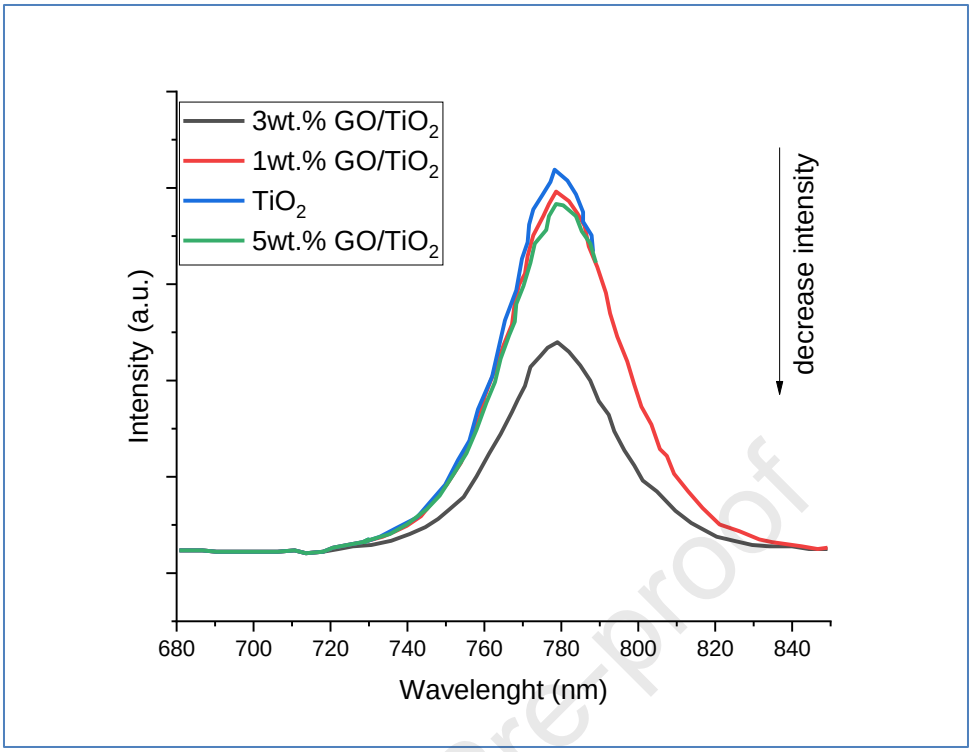

Fig. 9. PL spectrum of prepared electrodes.

Time-resolved photoluminescence (TRPL) analysis was measured to estimate the electron lifetime of the prepared electron transfer materials (ETMs) and the results are shown in Fig. 10. The spectrum was fitted to the function of tri-exponential (Eq. 2) and it showed the decay of lifetime in nanoseconds. This function contains a rapid decay lifetime component, which would generate from the charge carriers quenching that relocated to the electron contacts, while the two slow lifetime of decay component could be assign to the relative recombination of holes and electrons before collection of charges [42]. The average lifetimes of the prepared samples were calculated from Eq. 3 and the results are summarized in **Table2**.

Table2.TRPL decay measurements of TiO_2 and 3wt.% GO-TiO_2/$(FAPbI3)_{0.8}(MAPbBr3)_{0.2}$.

Perovskite/ETMs	τ_1 (ns)	τ_2 (ns)	A_1*	A_2*	$<\tau>$ (ns)

$TiO_2/(FAPbI_3)_{0.8}(MAPbBr_3)_{0.2}$	290	13	0.037	0.732	151
3wt.% GO-TiO_2NFs/$(FAPbI_3)_{0.8}(MAPbBr_3)_{0.2}$	86	19	0.026	0.626	52

The results indicate that the TiO_2 and 3wt.% GO-TiO_2 deposited on $(FAPbI_3)_{0.8}(MAPbBr_3)_{0.2}$-layer film electrodes demonstrate fast decay lifetimes of 290 and 86 ns (τ_1) respectively, while slow lifetimes of decay for respective electrodes are 13 and 19 ns (τ_2). The estimated fraction values A_1 of the fast decay of lifetimes are 0.037 and 0.026 for $TiO_2/(FAPbI_3)_{0.8}(MAPbBr_3)_{0.2}$ and 3wt.% GO-$TiO_2/(FAPbI_3)_{0.8}(MAPbBr_3)_{0.2}$ electrodes and 0.732 and 0.626 for A_2 of respective electrodes. These results suggest that electrons extractions from conduction bands of $(FAPbI_3)_{0.8}(MAPbBr_3)_{0.2}$ to CB of 3wt.% GO-TiO_2 is more effective relatively, as well as, it exposed that GO easies effective charge dissociation in the $(FAPbI_3)_{0.8}(MAPbBr_3)_{0.2}$ layer. In addition to, the TRPL measurements illustrated that the incorporating nanocomposite sample easies electron extraction capability from CB of $(FAPbI_3)_{0.8}(MAPbBr_3)_{0.2}$ layer to CB of 3wt.% GO-TiO_2.

Journal Pre-proof

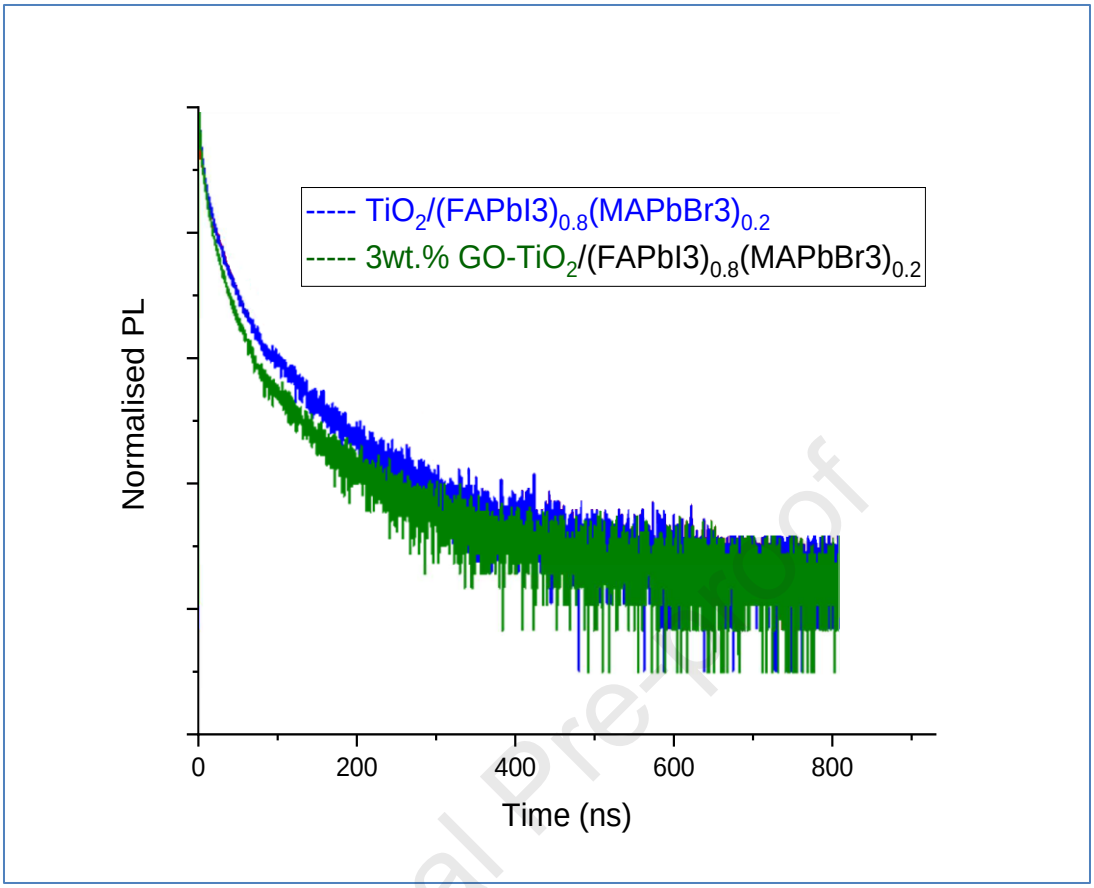

Fig. 10 TRPL of $TiO_2/(FAPbI3)_{0.8}(MAPbBr3)_{0.2}$ and 3wt.% GO-$TiO_2/(FAPbI_3)_{0.8}(MAPbBr_3)_{0.2}$.

3.4 Numerical investigation of solar cell

Beginning from the enter parameters of fabricated solar cell layers, the J-V properties of fabricated PVSC were emulated and paralleled to experimental data. A theoretical treatise of absorber defect density effect on the properties of PVSC is first carried out. The density defect is a substantial parameter that defines the electrical properties of PVSCs and, hence can assist to detect the efficiency [43]. In the range of 10^{14}-10^{17}, the effect results of defect densities on PVSC J-V properties are displayed in Fig. 11a. To detect the defect density that reproduce the experimental data, emulsion date or results were contrasted with experimental results. The defects density has a considerable effect on the value of VOC, were it reduce from 1.15V to

0.85V upon increase in defect density from 10^{14} to 10^{17} cm^{-1} without any impact of Jsc values, and these results are in agreement with reported results [44]. The experimental and theoretical calculation of J-V plot are presented in Fig. 11b. The results show that the calculations are in agreement with each other. The experimental and theoretical calculations appeared that conversion efficiency of power were 13.15% and 13.32% respectively. on the other hand, the quantum efficiency is another substantial property to investigate our numerical calculations, and the results are shown in Fig. 11c. The results obtained that the theoretical plot is in good agreement with experimental curve. As well as, form this plot, observed the contribution of electron-hole pairs that photogenerated in current density, where the experimental data appear 49% and 52% for theoretical data, which indicate that the half of photons fallen on PVSC are utilized in the process of conversion. From Fig 11b, c, its illustrated that the design model depend on recombination during defects is fit to demonstrate experimental data from QE and J-V data.

Journal Pre-proof

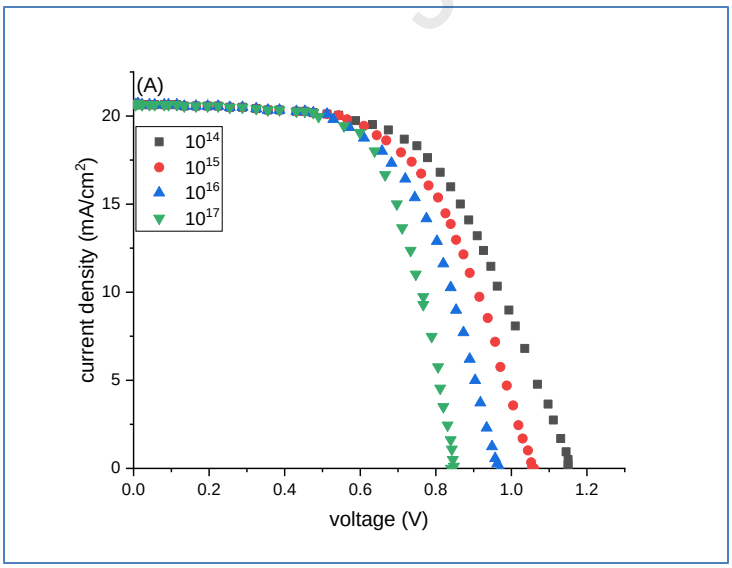

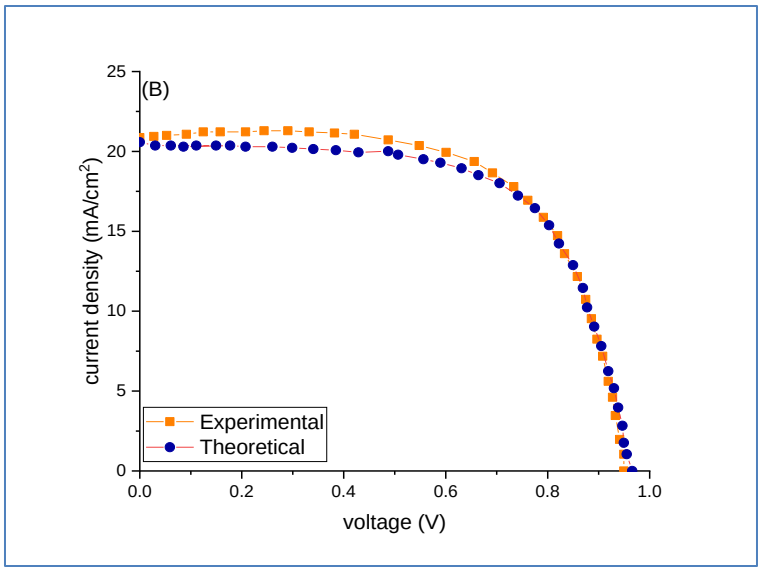

Journal Pre-proof

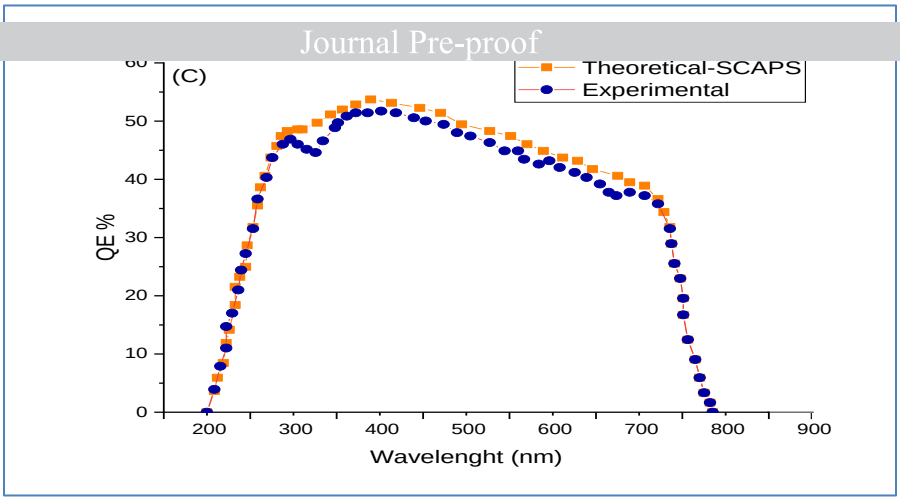

Fig. 11 (a) effect of defect density on J-V curves of fabricated PVSC, (b) J-V plots from theoretical validation and experimental on PVSC, (c) QE of theoretical and experimental on PVSC.

3.5 Photovoltaic measurements

Fig. 12a appear a graphical display of the perovskite system having Glass/ITO/3wt.%GO-TiO_2/$(FAPbI_3)_{0.8}(MAPbBr_3)_{0.2}$/MeOTAD/Ag arrangement utilized in this study. In fabricating PVSCs, $(FAPbI_3)_{0.8}(MAPbBr_3)_{0.2}$ absorber layer is sandwiched between TiO_2 block layer/ 3wt.%GO-TiO_2 that work as ETMs and spiro-MeOTAD HTMs. The SEM cross section image of fabricated PVSC is shown in Fig. 12b, where the thickness are 50, 130, 550, 200 and 70 nm for TiO_2, 3wt.%GO-TiO_2, $(FAPbI_3)_{0.8}(MAPbBr_3)_{0.2}$ capping layer, HTM and Ag respectively. The image is shown the production of $(FAPbI_3)_{0.8}(MAPbBr_3)_{0.2}$ capping layer with highly crystalline and pin-hole free on the 3wt.%GO-TiO_2 film and this layer separates of the spiro and TiO_2 electron transfer materials (HTMs). So, in this device, the ohmic contact between electrodes are little possibilities. The current-voltage (J-V) properties of prepared PVCS and it parameters are shown in Fig. 12c and summarized in **Table. 3**. In this report, we utilized four synthesized materials (TiO_2, 1wt.% GO-TiO_2, 3wt.% GO-TiO_2 and 5wt.% GO-TiO_2) as electron transporting materials (ETMs) and investigated its execution utilizing the $(FAPbI_3)_{0.8}(MAPbBr_3)_{0.2}$ as adsorbing layer of light. The results appeared that the device based on TiO_2 showed the efficiency less than device-based GO-TiO_2, which may be attributed to smaller grain size as

showed in FESEM results [45]. From results (**Table. 3**), the device based 1wt.% GO-TiO_2 shown VOCof 1.124 V, J_{SC} of 23.45 $mAcm^{-2}$, FF of 0.702 yielding PCE 18.50%, while in device based 3wt.% GO-TiO_2 exhibited VOCof 1.76 V, JSC of 24.06 $mAcm^{-2}$, FF of of 0.712 yielding PCE 20.14%. The difference in PEC% may be back to the fast transportation of electrons and low recombination of e^--h^+ [45]. In the case of 5wt.% GO-TiO_2 ETMs, the J-V results shown VOC of 1.133 V, JSC of 23.59 $mAcm^{-2}$, FF of 0.734 yielding PCE 19.61%. The decrease in efficiency emerges because of the high graphene oxide concentration and low grain size, and this causes decreasing in crystalline and hence difficultly in charge transport. All efficiency results are in agreement with PL spectrum results.

Table. 3. J-V of prepared materials based on $(FAPbI_3)_{0.8}(MAPbBr_3)_{0.2}$.

Perovskite/ETMs	VOC (V)	Jsc (mA/cm^2)	**FF**	**%PEC**
$TiO_2/(FAPbI_3)_{0.8}(MAPbBr_3)_{0.2}$	1.132	23.73	0.686	18.42
1wt.% GO-TiO_2NFs/$(FAPbI_3)_{0.8}(MAPbBr_3)_{0.2}$	1.124	23.45	0.702	18.50
3wt.% GO-TiO_2NFs/$(FAPbI_3)_{0.8}(MAPbBr_3)_{0.2}$	1.176	24.06	0.712	20.14
5wt.% GO-TiO_2NFs/$(FAPbI_3)_{0.8}(MAPbBr_3)_{0.2}$	1.133	23.59	0.734	19.61

Journal Pre-proof

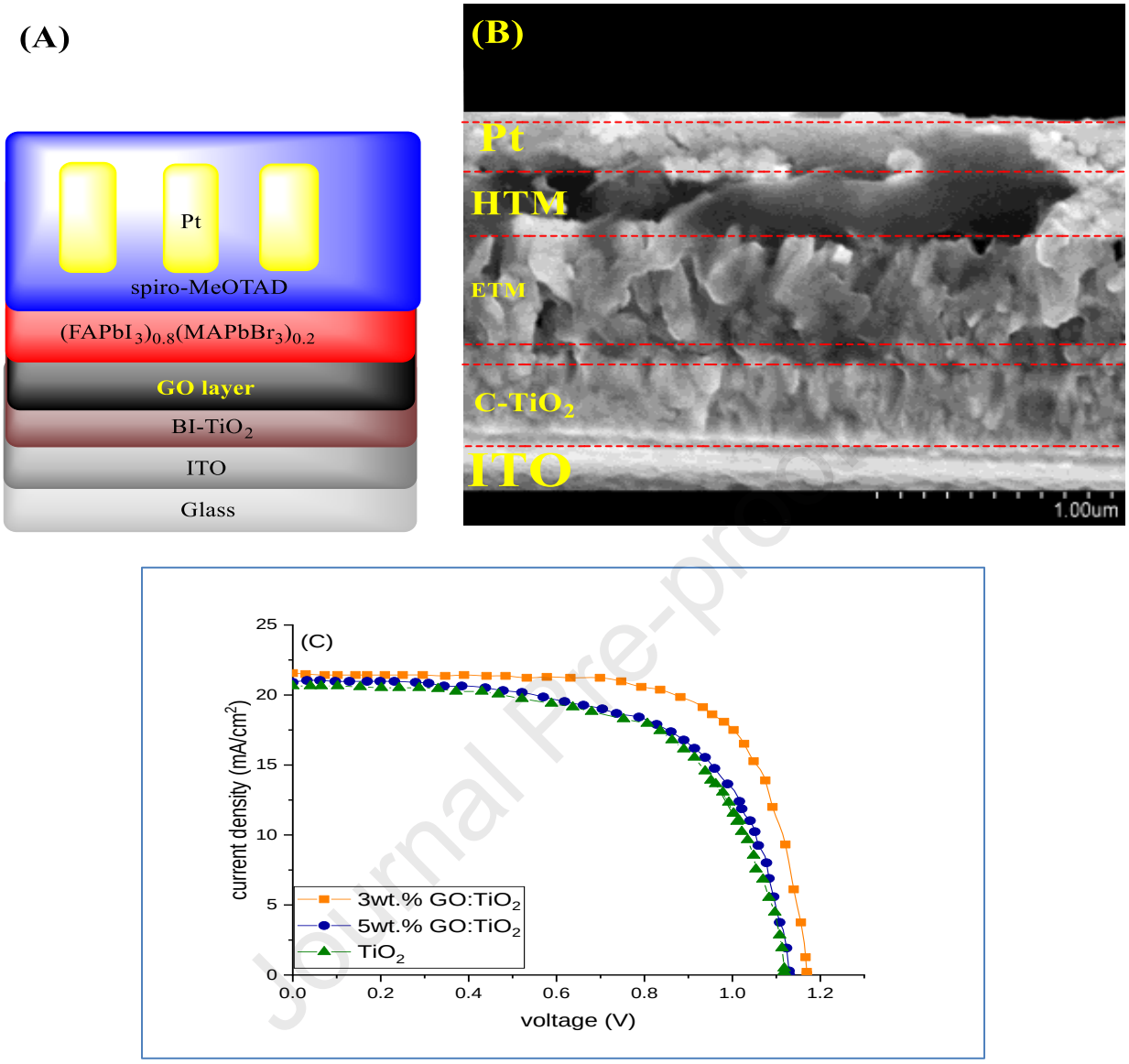

Fig. 12 (a) schematics device, (b) FESEM cross section of 3wt.% GO-TiO_2 based $(FAPbI_3)_{0.8}(MAPbBr_3)_{0.2}$ and (c) J-S curve of fabricated PVSCs.

To distinctly appear the pathway of charge transfer, the band gap diagram of ITO, TiO_2, GO-TiO_2, ETM and ETM was plotted on the bases of their edges of conduction band and energy gap as following:

Anatase TiO_2 (-4.0eV), ETM layer (-3.9eV), the HOMO level of ETM layer (-5.20eV) and (-4.3eV) for GO as shown in Fig. 13. The diagram shown the reduce or lower energy gap of GO

and this causes transfer the photoexcited electron from ETM layer and TiO_2 to GO. So, the GO/TiO_2 nanocomposite based PVSC should supply improved collection and charge transfer properties, as well as, a good performing wt.% GO/TiO_2 nanocomposite PVSC is fabricated via future controlling film thickness.

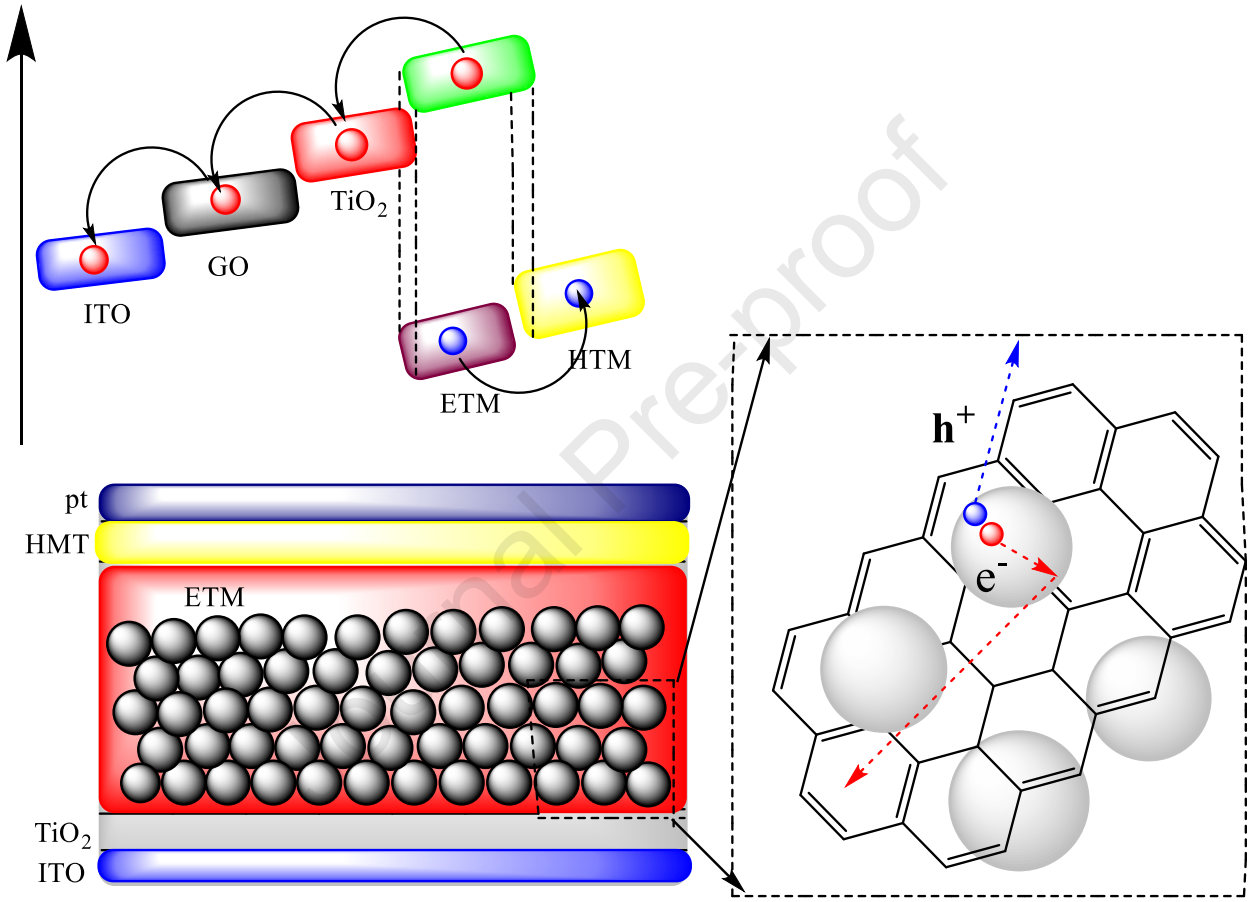

Fig. 13 Electron-hole transfer in fabricated PVSCs.

Comparing with previous reports (**Table 4**), this fabricated PVSCs showed a good Jsc, VOC, and efficiency.

Table. 4 Efficiency of PVSCs based on literature and comparison with this study.

Solar cell	Jsc (mA/cm^2)	VOC (V)	Efficiency (%)	References
1wt. GO-TiO_2	22.84	/	13.60%	[52]
GO-TiO_2	22.78	0.61	17.73%	[53]
0.4 vol.% rGO/TiO_2	21.00	0.91	13.5	[54]
GO/ TiO_2	1	1	2.50	[55]
$CH_3NH_3PbI_3/TiO_2$	20.0	0.98	12.00	[56]
$CH_3NH_3PbI_2Br/TiO_2$	10.12	0.82	4.80	[57]
TiO_2/(FAPbI3)0.8(MAPbBr3)0.2	1.13	23.73	18.42	Our study
3wt.% GO-TiO_2NFs/(FAPbI3)0.8(MAPbBr3)0.2	1.17	24.06	20.14	Our study

4 Conclusion

A series of wt.% GO-TiO_2 composite NFs high crystalline are synthesized by a electrospun method and deposited on boundary of $(FAPbI_3)_{0.8}(MAPbBr_3)_{0.2}$ perovskite and its photovoltaic activity is investigated. The effect of GO in TiO_2 NFs have been estimated in detail. The 3wt.% GO-TiO_2 composite NFs easies the limited centers of nuclei cause in highly uniform perovskite grain size. The implied effect of the 3wt.% GO-TiO_2 and mechanism were studied by TRPL analysis. The results of charges transfer exposed that GO easies better collection of charges and fast electron transportation, causes to a frequently ameliorated PEC. The optimized 3wt.% GO-TiO_2 composite NFs-based electron transfer materials obtained 20.14 % PCE with VOC 1.176 V, Jsc 24.06 mA/cm^2 and FF 0.712. The 3wt.% GO-TiO_2 could avail as an effective channel of electrons extraction and transfer from $(FAPbI_3)_{0.8}(MAPbBr_3)_{0.2}$ perovskite layer. The hybridization also improved the values of Jsc and VOC, leading to higher efficiency

transportation, as constructed to the TiO_2 nanoparticles. This novel synthesis method proposes an appropriate and friendly model to enhance the PVSC efficiency.

Data availability

All data generated or analyzed during this study are included in this published article

Declaration of Competing Interest

The authors declare that they have no known competing financial interests or personal relationships that could have appeared to influence the work reported in this paper.

Author contributions

Chou-Yi Hsu, H. N. K. AL-Salman, Hussein H. Hussein: Writing-first drat, Writing-review and editing, conceptualization, **Nizomiddin Juraev:** Formal analysis, Data curation; **Zaid H. Mahmoud:** Supervision; **Saeb Jasim Al-Shuwaili, Hanan Hassan Ahmed:** Investigation; **Ahmed Ali Ami, Nahed Mahmood Ahmed, Seitkhan Azat:** Writing-review and editing; **Ehsan Kianfar:** Supervision; Writing-review and editing**.**

References

[1] R. Dhanabal, S.R. Dey, Perovskite solar cells: recent progress and strategies developed for minimizing interfacial recombination, Front. Mater. Sci. 16, (2022). https://doi.org/10.1007/s11706-022-0595-7

[2] Mounesh, K. V. Yatish, Anup Pandith, Gaber E. Eldesoky and Bhari Mallanna Nagaraja, A novel MWCNT-encapsulated (2-aminoethyl)piperazine-decorated zinc(ii) phthalocyanine composite: development of an electrochemical sensor for detecting the antipsychotic drug promazine in environmental samples, Journal of Materials Chemistry B 11(44) (2023) 10692-10705.

[3] Sanakousar F. M., Vidyasagar C. C., Shikandar D. B., Mounesh, Viswanatha C. C., Gururaj Hosamani, Prakash K. and Manjunatha N. K., Dual catalytic activity of hexagonal Mg–Sr

Journal Pre-proof

codoped ZnO nanocrystals for the degradation of an industrial levafix olive reactive dye under sunlight and biosensing applications, React. Chem. Eng., 2023,8, 2566-2591.

[4] Y. Zhang, H. Liu, Y. Miao, J. Yang, J. Wen, High absorptivity of perovskite solar cell enhanced by metal grating, Optoelectron. Lett. 18 (2022) 658–661. https://doi.org/10.1007/s11801-022-2076-8

[5] J. Wang, X. Zhou, J. Ni, J. Guan, M. Hu, R. Wang, Y. Zhang, J. Li, H. Cai, J. Zhang, High-performance perovskite solar cell based on mesoporous TiO2 electron transport layer enabled by composite treatment strategy. J Mater Sci: Mater Electron. 32 (2021) 28417–28425. https://doi.org/10.1007/s10854-021-07221-6

[6] W. Wang, Y. He, L. Qi, High-efficiency colorful perovskite solar cells using TiO_2 nanobowl arrays as a structured electron transport layer, Sci. China Mater. 63 (2020) 35–46. https://doi.org/10.1007/s40843-019-9452-1

[7] D.Y. Son, J.G. In, H.S. Kim, N.G. Park, 11% Efficient Perovskite Solar Cell Based on ZnO Nanorods: An Effective Charge Collection System, J. Phys. Chem. C. 118 (2014) 16567-16573. https://doi.org/10.1021/jp412407j

[8] H.S. Kim, J.W. Lee, N. Yantara, P.P. Boix, S.A. Kul-Karni, S. Mhaisalkar, M. Gratzel, N.G. Park, High Efficiency Solid State Sensitized Solar Cell-Based on Submicrometer Rutile TiO2 Nanorod and CH3NH3PbI3 Perovskite Sensitizer, Nano Lett. 1 (2013) 2412-2417. https://doi.org/10.1021/nl400286w

[9] J.T. Wang, J.M. Ball, E.M. Barea, A. Abate, J.A. Alexander-webber, J. Huang, M. Saliba, I. Mora-Sero, J. Bisquert, H.J. naith, R.J. Nicholas, Low-Temperature Processed Electron Collection Layers of Graphene/TiO2 Nanocomposites in Thin Film Perovskite Solar Cells, Nano Lett. 14 (2014) 724-730 https://doi.org/10.1021/nl403997a.

[10] Y. Lv, P. Wang, B. Cai, Q. Ma, X. Zheng, Y. Wu, Q. Jiang, J. Liu, W.H. Zhang, Facile Fabrication Of SnO2 Nanorod Arrays Films as Electron Transporting Layer for Perovskite Solar Cells, Sol. RRL. 2 (2018). https://doi.org/10.1002/solr.201800133

Journal Pre-proof

[11] S.S. Mali, C.A. Betty, C.K. Hong, Synthesis of a nanostructured rutile TiO2 electron transporting layer via an etching process for efficient perovskite solar cells: impact of the structural and crystalline properties of TiO2, J. Mater. Chem. A. 5 (2017) 12340-12353. https://doi.org/10.1039/C7TA02822A

[12] X. Zhang, Z. Bao, X. Tao, H. Sun, W. Chen, X. Zhou, Sn-doped TiO2 nanorod arrays and application in perovskite solar cells, RSC Adv. 4 (2017) 64001–64005. https://doi.org/10.1039/C4RA11155A

[13] Y. Xiao, G. Han, Y. Li, M. Li, Y. Chang, J. Wu, Electrospun lead-doped titanium dioxide nanofibers and the in situ preparation of perovskite-sensitized photoanodes for use in high performance perovskite solar cells, J. Mater. Chem. A. 2 (2014) 16856-16862. https://doi.org/10.1039/C4TA03658A

[14] S.S. Mali, C.S. Shim, H.J. Kim, P.S. Patil, C.K. Hong, In situ processed gold nanoparticle-embedded TiO2 nanofibers enabling plasmonic perovskite solar cells to exceed 14% conversion efficiency. Nanoscale. 8 (2016) 2664–2677. https://doi.org/10.1039/C5NR07395B

[15] M. Saliba, W. Zhang, V.M. Burlakov, S.D. Stranks, Y. Sun, J.M. Ball, M.B. Johnston, A. Goriely, U. Wiesner, H.J. Snaith, Plasmonic-Induced Photon Recycling in Metal Halide Perovskite Solar Cells, Adv. Funct. Mater. 25 (2015) 5038-5046. https://doi.org/10.1002/adfm.201500669

[16] Q. Cui, X. Zhao, H. Lin, L. Yang, H. Chen, Y. Zhang, X. Li, Improved efficient perovskite solar cells based on Ta-doped TiO2 nanorod arrays. Nanoscale. 9 (2017) 18897–18907. https://doi.org/10.1039/C7NR05687G

[17] G. Yin, J. Ma, H. Jiang, J. Li, D. Yang, F. Gao, J. Zeng, Z. Liu, S.F. Liu, Enhancing efficiency and stability of perovskite solar cells through Nb-doping of TiO2 at low temperature. ACS Appl. Mater. Interfaces. 9 (2017) 10752–10758. https://doi.org/10.1021/acsami.7b01063

[18] S.S. Mali, J.V. Patil, H. Kim, C.K. Hong, Gallium Cationic Incorporated Compact TiO2 as an Efficient Electron-Transporting Layer for Stable Perovskite Solar Cells. Matter. 1 (2019) 1-13. https://doi.org/10.1016/j.matt.2019.04.001

Journal Pre-proof

[19] Y. Liu, G. Che, W. Cui, B. Pang, Q. Sun, L. Yu, L. Dong, Enhanced charge extraction for all-inorganic perovskite solar cells by graphene oxide quantum dots modified TiO2 layer, Front. Chem. Sci. Eng. 17 (2023) 516-524. https://doi.org/10.1007/s11705-022-2238-z

[20] K.T. Cho, G. Grancini, Y. Lee, D. Konios, S. Paek, E. Kymakis, M.K. Nazeeruddin, Beneficial Role of Reduced Graphene Oxide for Electron Extraction in Highly Efficient Perovskite Solar Cells, Nano Lett. 14 (2014) 14 724-730. https://doi.org/10.1002/cssc.201601070.

[21] J.T. Wang, J.M. Ball, E.M. Barea, A. Abate, J.A. Alexander-Webber, J. Huang, M. Saliba, I. Mora-Sero, J. Bisquert, H.J. Snaith, R.J. Nicholas, Low-Temperature Processed Electron Collection Layers of Graphene/TiO2 Nanocomposites in Thin Film Perovskite Solar Cells, ChemSusChem. 9 (2016) 3040-3044. https://doi.org/10.1021/nl403997a

[22] Z.H. Mahmoud, R.A. AL-Bayati, A.A Khadom, Synthesis and supercapacitor performance of polyaniline-titanium dioxide-samarium oxide (PANI/TiO2-Sm2O3) nanocomposite, Chem. Pap. 76 (2022) 1401–1412. https://doi.org/10.1007/s11696-021-01948-6

[23] Z.H. Mahmoud, R.A. AL-Bayati, A.A Khadom, Electron transport in dye-sanitized solar cell with tin-doped titanium dioxide as photoanode materials. J Mater Sci: Mater Electron. 33 (2022) 5009–5023. https://doi.org/10.1007/s10854-021-07690-9

[24] S.S. Mali, C.S. Shin, C.K. Hong, Highly stable and efficient solid-state solar cells based on methylammonium lead bromide (CH3NH3PbBr3) perovskite quantum dots, NPG Asia Mater, 7 (2015) 208. https://doi.org/10.1038/am.2015.86

[25] M.I. Saidaminov, A.L. Abdelhady, B. Murali, E. Alarousu, V.M. Burlakov, W. Peng, I. Dursun, L. Wang, Y. He, G. Maculan, A. Goriely, T. Wu, O.F. Mohammed, O.M. Bakr, High-quality bulk hybrid perovskite single crystals within minutes by inverse temperature crystallization, Nat. Commun. 6 (2015) 7586. https://doi.org/10.1038/ncomms8586

[26] Z.H. Mahmoud, R.A. AL-Bayati, A.A Khadom, Enhanced photovoltaic performance of dye-sanitized solar cell with tin doped titanium dioxide as photoanode materials, Chalcogenide Lett., 18 (2021).

Journal Pre-proof

[27] A.A. Kanouna, M.E. Benali Kanounb, A. Merada, S. Goumri-Said, Toward development of high performance perovskite solar cells based on CH3NH3GeI3 using computational approach. Sol. Energy, 182 (2019) 237–244. https://doi.org/10.1016/j.solener.2019.02.041.

[28] Y. Raoui, H. Ez-Zahraouy, N. Tahiri, O. El Bounagui, S. Ahmad, S. Kazim, Performance analysis of MAPbI3 based perovskite solar cells employing diverse charge selective contacts: Simulation study. Sol. Energy, 193 (2019) 948–955. https://doi.org/10.1016/j.solener.2019.10.009

[29] Z.H. Mahmoud, O.G. Hammoudi, A.N. Abd, Y.M. Ahmed, U.S. Altimari, A.H. Dawood, R. Shaker, Functionalize cobalt ferrite and ferric oxide by nitrogen organic compound with high supercapacitor performance, Results Chem. 5 (2023). https://doi.org/10.1016/j.rechem.2023.100936

[30] A. Kamada, T. Kuwahara, LHC lifetime frontier and visible decay searches in composite asymmetric dark matter models, J. High Energ. Phys.176 (2022). https://doi.org/10.1007/JHEP03(2022)176

[31] J. Xu, L. Wang, Y. Zhu, Decontamination of bisphenol A from aqueous solution by graphene adsorption. Langmuir, 28 (2012) 8418–8425. https://doi.org/10.1021/la301476p

[32] J. Yu, T. Ma, S. Liu, Enhanced photocatalytic activity of mesoporous TiO2 aggregates by embedding carbon nanotubes as electron-transfer channel, Phys. Chem. Chem. Phys. 133 (2011) 491–3501. https://doi.org/10.1039/C0CP01139H

[33] S. Perera, D. Perera, G. Ruperto, V. Khiem, N. Nijem, S. Oliver, C. Yves, J. Kenneth, Hydrothermal synthesis of graphene-TiO2 nanotube composites with enhanced photocatalytic activity, ACS Catal. 2 (2012) 949–956. https://doi.org/10.1021/cs200621c

[34] J. Sha, N. Zhao, E. Liu, C. Shi, C. He, J. Li, In situ synthesis of ultrathin 2-D TiO2 with high energy facets on graphene oxide for enhancing photocatalytic activity. Carbon, 68 (2014) 352–359. https://doi.org/10.1016/j.carbon.2013.10.087

[35] Z. Jia, F. Wang, B. Zhang, Simple Solvothermal routes to synthesize 3D BiOBrxI1-x microspheres and their visible-light-induced photocatalytic properties, Ind. Eng. Chem. Res. 50 (2011) 6688–6694. https://doi.org/10.1021/ie102310a

Journal Pre-proof

[36] H. Wang, F. Wang, Electrochemical investigation of an artificial solid electrolyte interface for improving the cycle-ability of lithium ion batteries using an atomic layer deposition on a graphite electrode. J Power Sources, 233 (2013) 1–5. https://doi.org/10.1016/j.jpowsour.2013.01.134

[37] R. Nehru, Y. Hsu, S. Wang, Graphene oxide@Ce-doped TiO2 nanoparticles as electrocatalyst materials for voltammetric detection of hazardous methyl parathion. Microchim Acta, 188 (2021). https://doi.org/10.1007/s00604-021-04847-5

[38] M. Ahmadian-Yazdi, M. Eslamian, Toward scale-up of perovskite solar cells: Annealing-free perovskite layer by low-cost ultrasonic substrate vibration of wet Films, Mater. Today Commun. 14 (2018) 151-159. https://doi.org/10.1016/j.mtcomm.2018.01.006

[39] T. Bindu Sharmila, A. Nair, B. Abraham, P. Beegum, E. Thachil, Microwave exfoliated reduced graphene oxide epoxy nanocomposites for high performance application. Polymer, 55 (2014). https://doi.org/10.1016/j.polymer.2014.05.032

[40] J. Patil, S. Mali, J. Shaikh, A. Patil, P. Patil, C. Hong, Influence of reduced graphene Oxide-TiO2 composite nanofibers in organic indoline DN350 based dye sensitized solar cells, Synth. Met. 256 (2019). https://doi.org/10.1016/j.synthmet.2019.116146

[41] S. Mali, H. Kim, J. Patil, C. Hong, Bio-inspired Carbon Hole Transporting Layer Derived from Aloe Vera Plant for Cost-Effective Fully Printable Mesoscopic Carbon Perovskite Solar Cells. ACS Appl. Mater. Interfaces, 10 (2019) 31280-31290. https://doi.org/10.1021/acsami.8b08383

[42] Y. Ma, P. Hangoma, W. Park, J. Lim, Y. Jung, J. Jeong, S. Park, K. Kim, Controlled crystal facet of MAPbI3 perovskite for highly efficient and stable solar cell via nucleation modulation. Nanoscale, 11 (2019) 170-177. https://doi.org/10.1039/C8NR08344D

[43] T. Minemoto, M. Murata, Theoretical analysis on effect of band offsets in perovskite solar cells, Sol. Energy Mater. Sol. Cells. 133 (2015) 8–14. https://doi.org/10.1016/j.solmat.2014.10.036

Journal Pre-proof

[44] C. Ran, J. Xu, W. Gao, C. Huang, S. Dou, Defects in metal triiodine perovskite materials towards high-performance solar cells: origin, impact, characterization, and engineering, Chem. Soc. Rev. 47 (2018) 4581–4610. https://doi.org/10.1039/C7CS00868F

[45] R. Brüninghoff, K. Wenderich, J.P. Korterik, B.T. Mei, G. Mul, A. Huijser, Time-Dependent Photoluminescence of Nanostructured Anatase TiO2 and the Role of Bulk and Surface Processes, J. Phys. Chem. C. 123 (2019) 26653–26661. https://doi.org/10.1021/acs.jpcc.9b06890.

[46] Al-Salman, H. N. K., sabbar Falih, M., Deab, H. B., Altimari, U. S., Shakier, H. G., Dawood, A. H., ... & Kianfar, E. (2023). A study in analytical chemistry of adsorption of heavy metal ions using chitosan/graphene nanocomposites. Case Studies in Chemical and Environmental Engineering, 8, 100426.

[47] Ghobad Behzadi pour, Elahe Shajee nia, Elham Darabi, Leila Fekri aval, Hamed Nazarpour-Fard, Ehsan Kianfar, Fast NO2 gas pollutant removal using CNTs/TiO2/CuO/zeolite nanocomposites at the room temperature,Case Studies in Chemical and Environmental Engineering, Volume 8,2023,100527,https://doi.org/10.1016/j.cscee.2023.100527.

[48] Hsu, C. Y., Rheima, A. M., Mohammed, M. S., Kadhim, M. M., Mohammed, S. H., Abbas, F. H., ... & Mahmoud, Z. H. (2023). Application of Carbon Nanotubes and Graphene-Based Nanoadsorbents in Water Treatment. BioNanoScience, 1-19.

[49] sabri Abbas, Z., Kadhim, M. M., Mahdi Rheima, A., jawad al-bayati, A. D., Talib Abed, Z., dashoor Al-Jaafari, F. M., ... & Kianfar, E. (2023). Preparing Hybrid Nanocomposites on the Basis of Resole/Graphene/Carbon Fibers for Investigating Mechanical and Thermal Properties. BioNanoScience, 1-29.

[50] Smaisim, G. F., Abed, A. M., Al-Madhhachi, H., Hadrawi, S. K., Al-Khateeb, H. M. M., & Kianfar, E. (2023). Graphene-based important carbon structures and nanomaterials for energy storage applications as chemical capacitors and supercapacitor electrodes: A review. BioNanoScience, 13(1), 219-248.

Journal Pre-proof

[51] Salahdin, O. D., Sayadi, H., Solanki, R., Parra, R. M. R., Al-Thamir, M., Jalil, A. T., ... & Kianfar, E. (2022). Graphene and carbon structures and nanomaterials for energy storage. Applied Physics A, 128(8), 703.

[52] Yang, H., Liu, N., Ran, M. et al. Enhancing electron transport in perovskite solar cells by incorporating GO to the meso-structured TiO2 layer. J Mater Sci: Mater Electron 31, 3603–3612 (2020). https://doi.org/10.1007/s10854-020-02913-x

[53] Weizhong Liang, Yongsong Zhang, Jian Xiong, Xiaoying Huang, Yunfei Xu, Lu Zhang, Yujun Zhou, Siyu liu, Weizhi Liu, Naihe Liu, Junqian Dai, Yu Huang, Zheling Zhang, Zhen He, Jian Zhang, Synthesis of highly dispersed TiO2 NPs/GO composites sol and its application in inverted perovskite solar cells, Organic Electronics, https://doi.org/10.1016/j.orgel.2022.106616.

[54] Gill Sang Han, Young Hyun Song, Young Un Jin, Jin-Wook Lee, Nam-Gyu Park, Bong Kyun Kang, Jung-Kun Lee, In Sun Cho, Dae Ho Yoon, and Hyun Suk Jung, Reduced Graphene Oxide/Mesoporous TiO2 Nanocomposite Based Perovskite Solar Cells, ACS Applied Materials & Interfaces, http://doi.org/10.1021/acsami.5b06171.

[55] Hmoud Al Dmour, SCAPS Numerical Analysis of Graphene Oxide /TiO2 Bulk Heterojunction Solar Cell Sensitized byN719 Ruthenium Dye, East European Journal of Physics, https://doi.org/10.26565/2312-4334-2023-3-65

[56] H. Heo, S. H. Im, J. H. Noh, T. N. Mandal, C. S. Lim, J. A. Chang, Y. H. Lee, H. J. Kim, A. Sarkar, Md. K. Nazeeruddin, M. Grätzel and S Il. Seok, Nature Photon. 2013, 7, 486.

[57] Qiu, J., Qiu, Y., Yan, K., Zhong, M., Mu, C., Yan, H., & Yang, S. (2013). All-solid-state hybrid solar cells based on a new organometal halide perovskite sensitizer and one-dimensional TiO2 nanowire arrays. Nanoscale, 5(8), 3245-3248.

[58] Baqaei, A., Sabbagh Alvani, A. A., Sameie, H., & Rosei, F. (2023). Role of pH in the hydrothermal synthesis of TiO2 nanorod photocatalysts. ChemistrySelect, 8(25), e202300792.

[59] Baqaei, A., Alvani, A. A. S., & Sameie, H. (2022). Enhancement of visible-light photo-activity of TiO2 arrays for environmental water purification. Pigment & Resin Technology, (ahead-of-print).

Journal Pre-proof

[60] Baqaei, A., Sabbagh Alvani, A. A., & Sameie, H. (2022). Preparation of One-dimensional Reduced Titanium Dioxide; A Candidate for photocatalytic Applications. Advanced Materials and New Coatings, 10(39), 2872-2880.

[61] Sameie, H., Alvani, A. S., Mei, B. T., Salimi, R., Poelman, D., & Rosei, F. (2021). Mo-doped ZnV2O6/reduced graphene oxide photoanodes for solar hydrogen production. Electrochimica acta, 382, 138333.

[62] Golmohammadi, M., Sabbagh Alvani, A., Sameie, H., & Salimi, R. (2019). Characterization of photocatalytic nanocomposites contains reduced graphene oxide and polymeric membrane for dye degradation purpose. Journal of Studies in Color World, 9(1), 13-22.

[63] Baghaei, A., Sabbagh Alvani, A. A., Sameie, H., & Salimi, R. (2019). Effect of temperature in hydrothermally rutile TiO2 nanorod synthesis for photocatalytic applications. Journal of Color Science and Technology, 12(4), 251-259.

[64] Izadi, M., Mardani, H., Roghani-Mamaqani, H., & Salami-Kalajahi, M. (2022). Hybrid composites of epoxidized polyurethane and novolac resins cured by poly (amidoamine) dendrimer-grafted graphene oxide. Polymer Bulletin, 79(8), 5975-5990.

[65] Hamrahjoo, M., Hadad, S., Dehghani, E., Salami-Kalajahi, M., & Roghani-Mamaqani, H. (2022). Poly (poly [ethylene glycol] methyl ether methacrylate)/graphene oxide nanocomposite gel polymer electrolytes prepared by controlled and conventional radical polymerizations for lithium ion batteries. International Journal of Energy Research, 46(7), 9114-9127.

[66] Easavinejad, H., Mardani, H., Roghani-Mamaqani, H., & Salami-Kalajahi, M. (2022). Preparation of silica-decorated graphite oxide and epoxy-modified phenolic resin composites. Fullerenes, Nanotubes and Carbon Nanostructures, 30(3), 348-357.

[67] Izadi, M., Mardani, H., Roghani-Mamaqani, H., Salami-Kalajahi, M., & Khezri, K. (2021). Hyperbranched Poly (amidoamine)-Grafted Graphene Oxide as a Multifunctional Curing Agent for Epoxy-Terminated Polyurethane Composites. ChemistrySelect, 6(11), 2692-2699.

Journal Pre-proof

[68] Shokri, A. A., Talebi, S., & Salami-Kalajahi, M. (2020). Polybutadiene Rubber/Graphene Nanocomposites Prepared via In Situ Coordination Polymerization Using the Neodymium-Based Ziegler–Natta Catalyst. Industrial & Engineering Chemistry Research, 59(34), 15202-15213.

[69] Hsu, C. Y., Mahmoud, Z. H., Abdullaev, S., Ali, F. K., Naeem, Y. A., Mizher, R. M., ... & Habibzadeh, S. (2024). Nano titanium oxide (nano-TiO2): A review of synthesis methods, properties, and applications. Case Studies in Chemical and Environmental Engineering, 100626.

[70] Ajaj, Y., AL-Salman, H. N. K., Hussein, A. M., Jamee, M. K., Abdullaev, S., Omran, A. A., ... & Mahmoud, Z. H. (2024). Effect and investigating of graphene nanoparticles on mechanical, physical properties of polylactic acid polymer. Case Studies in Chemical and Environmental Engineering, 100612.

[71] Al-Salman, H. N. K., Hsu, C. Y., Jawad, Z. N., Mahmoud, Z. H., Mohammed, F., Saud, A., ... & Kianfar, E. (2023). Graphene oxide-based biosensors for detection of lung cancer: A review. Results in Chemistry, 101300.

[72] Fattahi, M., Hsu, C. Y., Ali, A. O., Mahmoud, Z. H., Dang, N. P., & Kianfar, E. (2023). Severe plastic deformation: Nanostructured materials, metal-based and polymer-based nanocomposites: A review. Heliyon.

[73] López-Covarrubias, J. G., Soto-Muñoz, L., Iglesias, A. L., & Villarreal-Gómez, L. J. (2019). Electrospun nanofibers applied to dye solar sensitive cells: A review. Materials, 12(19), 3190.

[74] Rahmati, M., Mills, D. K., Urbanska, A. M., Saeb, M. R., Venugopal, J. R., Ramakrishna, S., & Mozafari, M. (2021). Electrospinning for tissue engineering applications. Progress in Materials Science, 117, 100721.

[75] B. Bai, T. Xu, Q. Nie, and P. Li, "Temperature-driven migration of heavy metal Pb2+ along with moisture movement in unsaturated soils," International Journal of Heat and Mass Transfer, vol. 153, p. 119573, 2020.

[76] B. Bai, F. Bai, Q. Nie, and X. Jia, "A high-strength red mud–fly ash geopolymer and the implications of curing temperature," Powder Technology, vol. 416, p. 118242, 2023.

Journal Pre-proof

[77] B. Bai, J. Wang, Z. Zhai, and T. Xu, "The penetration processes of red mud filtrate in a porous medium by seepage," Transport in Porous Media, vol. 117, pp. 207-227, 2017.

[78] Wei, N., Yin, L., Yin, C., Liu, J., Wang, S., Qiao, W., & Zeng, F. (2023). Pseudo-correlation problem and its solution for the transfer forecasting of short-term natural gas loads. Gas Science and Engineering, 119, 205133. https://doi.org/10.1016/j.jgsce.2023.205133.

[79] Bing Bai, Fan Bai, Xianke Li, Qingke Nie, Xiangxin Jia, Haiyan Wu. The remediation efficiency of heavy metal pollutants in water by industrial red mud particle waste. https://doi.org/10.1016/j.eti.2022.102944.

[80] Sajjadnejad, M., Karkon, S., Haghshenas, S. M. S. (2024). 'Corrosion Characteristics of Zn-TiO2 Nanocomposite Coatings Fabricated by Electro-Codeposition Process', Advanced Journal of Chemistry, Section A, 7(2), 209-226. doi: 10.48309/ajca.2024.418391.1425.

[81] Ahmadlouydarab, M., Javadi, S., Adel Alijan Darab, F. (2023). 'Evaluation of Thermal Stability of TiO2 Applied on the Surface of a Ceramic Tile to Eliminate Methylene Blue Using Silica-based Doping Materials', Advanced Journal of Chemistry, Section A, 6(4), 352-365. doi: 10.22034/ajca.2023.405496.1379.

[82] Arjomandi Rad, F., Talat Mehrabad, J., Dizaji Esrafili, M. (2023). 'A Communal Experimental and DFT Study on Structural and Photocatalytic Properties of Nitrogen-Doped TiO2', Advanced Journal of Chemistry, Section A, 6(3), 244-252. doi: 10.22034/ajca.2023.391772.1358.

[83] Zaid Almarbd, Z., Mutter Abbass, N. (2022). 'Recycling of Plastic Waste Made of Polystyrene and Its Transformation into Nanocomposites by Green Methods', Chemical Methodologies, 6(12), 940-952. doi: 10.22034/chemm.2022.359620.1603.

[84] Al Taee, M. B., Al Shabander, B. M. (2022). 'Study the Effect of ZnO Concentrations on The Photocatalytic Activity of TiO2/Cement Nanocomposites', Chemical Methodologies, 6(11), 831-841. doi: 10.22034/chemm.2022.352379.1578.

Journal Pre-proof

[85] Moayeripour, S. S., Behzadi, R. (2023). 'Experimental investigation of the effect of titanium nano-particles on the properties of hydrophobic self-cleaning film', Journal of Medicinal and Pharmaceutical Chemistry Research, 5(4), 303-316.

[86] Daliri Shamsabadi, O. (2024). 'Investigation of Antimicrobial Effect and Mechanical Properties of Modified Starch Films, Cellulose Nanofibers, and Citrus Essential Oils by Disk Diffusion Method', Asian Journal of Green Chemistry, 8(1), 1-14. doi: 10.48309/ajgc.2024.398370.1394.

[87] Sabaghi, V., Jalaly, M., Rahsepar, F. (2020). 'Photocatalytic degradation of industrial pigments by mil-125 derived porous Titanium Dioxide (TiO2) nanoparticles', Journal of Medicinal and Nanomaterials Chemistry, 2(4), 300-312. doi: 10.48309/JMNC.2020.4.4.

[88] Allaedini, G., Tasirin, S. M. (2019). 'Comparison of TiO2 nanoparticles impact with TiO2/CNTs nano hybrid on microbial community of staphylococcus', Journal of Medicinal and Nanomaterials Chemistry, 1(4), 421-424. doi: 10.48309/JMNC.2019.4.5.

[89] Ambaraka, M. F., Aljazwia, F. M., Alsupikhe, R. F. (2019). 'Comparative investigations of synthesis TiO2 Nano-Particles from four different types of alcohols by Sol-Gel method and evaluation of their antibacterial activity', Journal of Medicinal and Nanomaterials Chemistry, 1(4), 431-438. doi: 10.48309/JMNC.2019.4.7.

[90] Malumi, S. O., Malumi, T., Osiele, M. O., Ekpekpo, A., Ikhioya, I. L. (2023). 'Enhance and Performance Evolution of Silver-Doped Titanium Dioxide Dye-Sensitized Solar Cells Using Different Dyes', Journal of Engineering in Industrial Research, 4(4), 189-200. doi: 10.48309/jeires.2023.4.1.

[91] Jiménez-Pérez, V. M., & Prakash, K. (2023). Thermal decomposition synthesis of cylindrical rod-like MoO3 and irregular sphere-like Ag2MoO4 nanocrystals for accelerating photocatalytic degradation of industrial reactive dyes and biosensing application. Journal of Environmental Chemical Engineering, 11(2), 109371.

[92] Mounesh, Reddy, K. V., Pandith, A., Eldesoky, G. E., & Nagaraja, B. M. (2024). Novel nitrogen-rich anchored nickel (II) phthalocyanine with composite of multiwalled carbon

nanotubes on modified glassy carbon electrode: Sensitive and selective electrocatalytic activity of nitrite. Applied Organometallic Chemistry, 38(1), e7302.

Journal Pre-proof

Journal Pre-proof

Declaration of Competing Interest

The authors declare that they have no known competing financial interests or personal relationships that could have appeared to influence the work reported in this paper.

Journal Pre-proof